IOWA STATE UNIVERSITY
Digital Repository

2015

An experimental study on the near wake characteristics of a wind turbine model subjected to surge, pitch, and heave motions

Morteza Khosravi
Iowa State University

**An experimental study on the near wake characteristics of a wind turbine model
subjected to surge, pitch, and heave motions**

by

Morteza Khosravi

A thesis submitted to the graduate faculty

in partial fulfillment of the requirements for the degree of

MASTER OF SCIENCE

Major: Aerospace Engineering

Program of Study Committee:
Hui Hu, Co-major Professor
Partha Sarkar, Co-major professor
Anupam Sharma

Iowa State University

Ames, Iowa

2015

DEDICATION

I dedicate this thesis to my beloved wife, Anastasiia, who patiently and positively encouraged me throughout my entire time as a graduate student, so that I could finish this research work and close this chapter of my life rapidly and more successfully. I would also like to dedicate this thesis to my wonderful son, Parsa who brings joy and happiness to my life, to my parents, siblings, and all those who have somehow cared, helped, and supported me during all this time as a graduate student. Thank you all.

TABLE OF CONTENTS

ACKNOWLEDGEMENTS

ABSTRACT

There are many advantages in floating wind turbines in deep waters, however, there are also significant technological challenges associated with it too. The dynamic excitation of wind and waves can induce excessive motions along each of the 6 degrees of freedom (6-DOF) of the floating platforms. These motions will then be transferred to the turbine, and directly impact the wake characteristics of the floating wind turbines, and consequently the resultant wind loadings and performances of the wind turbines sited in offshore wind farms.

In the present study, a comprehensive experimental study was performed to analyze the near wake characteristics of a wind turbine model subjected to surge, heave, and pitch motions. The experimental study was performed in a large-scale atmospheric boundary layer wind tunnel with a scaled three-blade Horizontal Axial Wind Turbine model placed in a turbulent boundary layer airflow with similar mean and turbulence characteristics as those over a typical offshore wind farm. The base of a 1:300 scaled model wind turbine was mounted on a translation stage. The translation stage can be controlled to generate surge, pitch and heave motions to simulate the dynamic motions experienced by floating offshore wind turbines. During the experiments, the velocity scaling method was chosen to maintain the similar velocity ratios (i.e., the ratios of the incoming airflow flow to that of turbine base motion) between the model and the prototype.

During the experiments, a high resolution digital particle image velocimetry (PIV) system was used to achieve flow field measurements to quantify the characteristics of the turbulent vortex flow in the near wake of the wind turbine model. Besides conducting ''free run'' PIV measurements to determine the ensemble-averaged statistics of the flow quantities such as mean velocity, Reynolds stress, and turbulence kinetic energy (TKE)

distributions in the wake flow, ''phase-locked'' PIV measurements were also performed to elucidate further details about evolution of the unsteady vortex structures in the wake flow in relation to the position of the rotating turbine blades. The effects of the surge, heave, and pitch motions of the wind turbine base on the wake flow characteristics were examined in great details based on the PIV measurements. The findings derived from the present study can be used to improve the understanding of the underlying physics for optimal mechanical design of floating offshore wind turbines, as well as the layout optimization of floating offshore wind farms.

The results of the wake study reveal that the wake of a wind turbine subjected to base motions, is highly dependent on which direction the turbine is oscillating. Furthermore, the velocity, frequency, and the range of oscillation also play an important role on the behavior and the wake pattern of the moving turbine.

In the case of the surge and pitch motions, the wake accelerates as the turbine is moving with the flow, hence, reducing the power extraction by the turbine. A decrease in Reynolds shear stress and the turbulent kinetic energy production was noted as the turbine was oscillating with the flow. However, as the turbine was moving into the flow, these effects reverse, and causes a deceleration in the wake of the moving turbine, hence increases the power production by the turbine, and increases the Reynolds shear stress and the turbulent kinetic energy.

In the case of the heave motion, the wake tends to shift upward as the turbine was moving downward and vice versa. However, no significant difference in the Reynolds shear stress and the T.K.E. between the wake of the bottom fixed turbine and the oscillating turbine in heave motion was noted.

CHAPTER 1

GENERAL INTRODUCTION

1.1 Offshore Wind Energy

Wind has the capability of becoming a major contributor in the world's energy production. In the United States, the production of electricity through onshore wind has already become one of the fastest growing energy sources. The increasing popularity of using wind as a renewable source of energy is in response to the limited supply of fossil fuels, environmental concerns over the use of non-renewable energy sources, and to reduce our dependence on foreign oil (MANWELL, 2012).

Due to the availability of suitable lands with higher wind speeds, the middle portion of the U.S. provides a unique condition for onshore wind farm developments. Although the wind resource in this area has the potential of providing substantial amount of clean energy for the entire nation, but the challenges associated with transporting this generated electricity to higher demand areas of the coastal regions would put a limit on how much electricity can actually be produced in this part of the country (Jonkman, 2007).

Wind turbines can also be installed offshore. Offshore wind energy is one of the most abundant and promising sources of energy that can provide substantial amount of clean, domestic, and renewable energy. The United States is especially fortunate to be surrounded by vast waters on both sides of the nation. This provides a unique opportunity for offshore wind farm developments in this country. There is over 4000 GW of wind potential within 50 nautical miles of the U.S. coastlines (Musial et al, 2010). The abundant U.S. offshore wind resources have the potential of powering the high populated areas in the coastal

regions where the energy cost and demand is much higher than many other locations in the United States. Figure 1, illustrates the average U.S. wind speeds for both onshore and offshore cases, along with the U.S. bathymetry distribution.
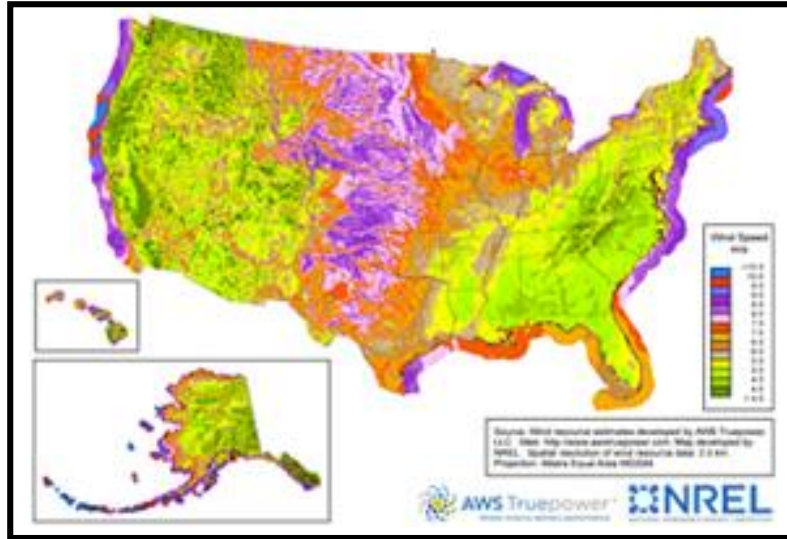
(a)
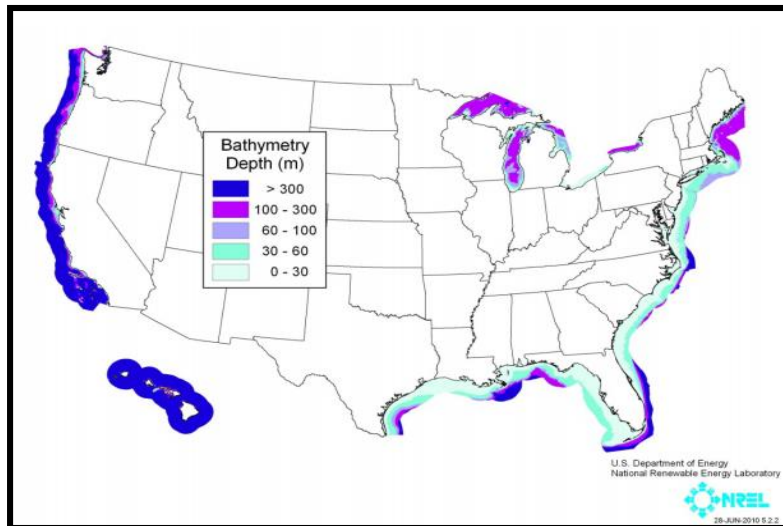
(b)

Figure 1: The U.S. wind resources for onshore and offshore (a), and the bathymetry distribution (b)
(http://apps2.eere.energy.gov/wind/windexchange/)

Although, offshore wind farms have many advantages over their onshore counterparts, but the most promising feature of an offshore wind farm is the vast availability of areas for such activities, considering 71% of the Earth is covered by water. This allows for large scale developments usually in the range of 1 GW near the load centers of coastal regions. (Hau, E.)

Other advantages include, but not limited to:

- The wind farms can be placed close enough to the shore so that transporting the generated electricity will not be costly or difficult, and at the same time they can be placed far enough offshore so that the visual and sound pollutions will not impact the coastal residents.

- The size of the offshore wind turbines are not limited by inland transportation constraints assuming the turbines can be manufactured near the coasts, and therefore multi megawatt turbines usually in the range of 5-10MW can easily be installed offshore.

- Stronger and steadier wind speeds at lower altitudes can provide an opportunity for reducing the tower heights while maintaining or perhaps increasing the energy output.

- The lower turbulence intensities offshore than onshore results in less fatigue loads on the turbine components, hence reducing the cost of O&M.

As shown in Figure 2, offshore wind energy is divided into three categories, depending on the depth of water where the turbines are being installed. The depth of the water dictates the type of substructure technology needed to install the offshore wind turbines. In shallow waters (0 m to 30 m), the turbines are being fixed to the sea floor by means of a monopile

or gravity based foundations. In intermediate waters (30m to 60 m), the wind turbines are also being fixed to the sea floor but by different kind of substructures such as jacket or tripods. As the water depth increases beyond 60m, the cost of substructure increases substantially, making it almost economically infeasible to fix the turbines to the sea floor. Therefore, the turbines will need to be floated in deep waters.
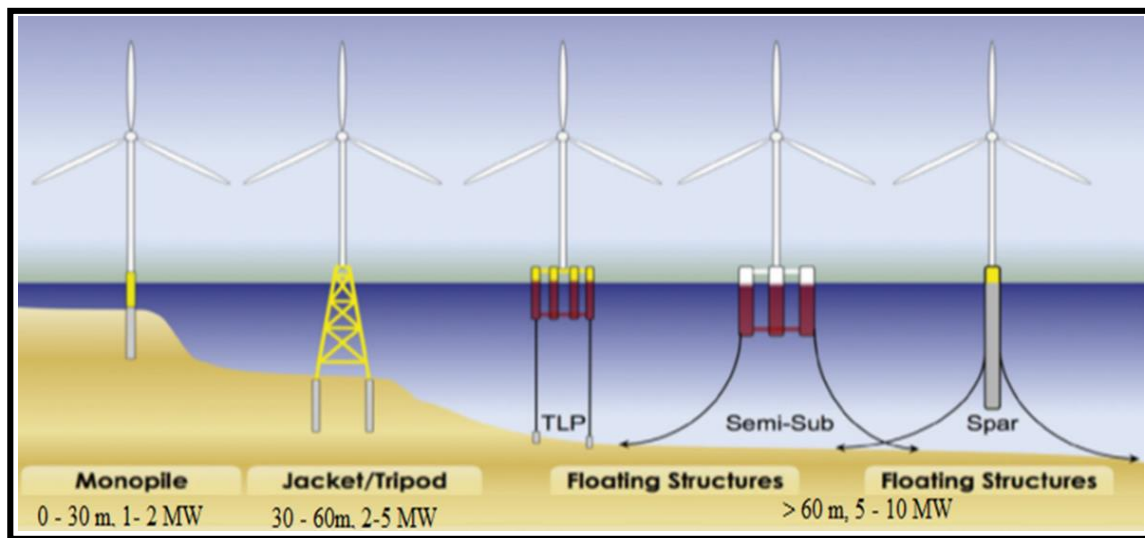
Figure 2: Progression of offshore wind turbines with increasing depth of water

By the end of 2014, there were 74 offshore wind farms operating in 11 European countries, yielding over 8 GW of electricity. All of these wind farms are located in shallow waters with depths less than 20 meters where the turbines are fixed to the sea floor (Corbetta G., 2015). Unlike the shallow European waters, the U.S. waters are, on the other hand, mostly deep (with the exception of a few regions in the East Coast and the Gulf of Mexico). Therefore, offshore wind farm development in the U.S. will most likely be based on the floating concept.

As shown in Figure 3, there are six degrees of freedom (6-DOF) associated with any floating structures, three in displacements (surge, sway, and heave) and three in rotations (roll, pitch, and yaw).
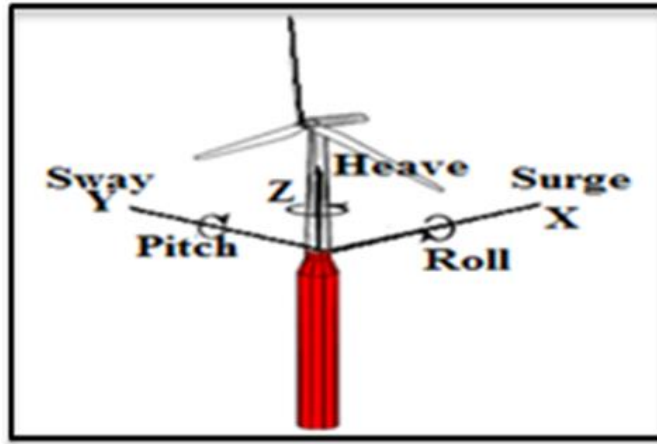

Figure 3: Degrees of freedom associated with a floating turbine

There are many advantages of floating wind turbines in deep waters. However, there are also significant technological challenges associated with it too.

The floating platforms that have been proposed for floating wind turbines include; semi-submersible, tension leg platform, and spar buoy. However, regardless of the type, floating platforms cannot easily provide high degrees of stability for mounting wind turbines. This is especially true for the Horizontal Axis Wind Turbines (HAWT). For a HAWT system, the mass of the floater is of the same order of magnitude as the mass of the nacelle and rotor assembly, and therefore, the center of gravity (C.G.) of a HAWT system is located at a much higher location in relation to their Center of Buoyancy (C.B.), hence, creating an unstable floating structure. Therefore, any external forces seen by the floater, will influence the rotor assembly, and any forces felt by the rotor assembly will be affecting the floater system.

In reality, any floating structure would need to be secured and mounted to the seafloor by means of mooring lines or tendons. The mooring lines are used to keep the turbines in place, and at the same time they increase the stability of the floating structure. The mooring line stability is achieved because, as the floating structure is being impacted by the external loading such as wind, wave, current, and etc., displacing the whole structure. As a result of this displacement, the mooring lines would go into high tensions. The high tensioned lines, would have two components. The horizontal component of the tension force, would be opposing the external loads, bringing the turbine to its original location. While, the vertical component of the tension force in the mooring lines, would be pointing downward, lowering the C.G. of the structure and bringing it closer to the C.B. hence, stabilizing the structure.

The dynamic excitation of wind and waves will induce excessive motions along each of the 6 degrees of freedom (6-DOF) of the floating platforms. These motions will then be transferred to the turbine, and directly impact the turbines' performance, loading and consequently, the wake characteristics of the floating wind turbines. Both coupled and uncoupled motion study of the floating turbines are important and necessary, in order to determine the contributions of each motions along each of the DOFs to the overall performance, loading, and the wake characteristics of floating wind turbines. However, the current study focuses only on the effects of the uncoupled base motions on the performance and the near wake behavior of the oscillating turbine.

The current study considers only the effects of the floater motions (base motions) on the performance, loading, and the near wake behavior of a horizontal axis wind turbine.

1.2 Atmospheric Physics

The atmosphere is in motion at all times. The layer of atmosphere in close vicinity of a surface, whose velocity is affected by the viscous shear is called atmospheric boundary layer (ABL). A one-dimensional development of boundary layer on a flat plate is shown in Figure 4.

At any instant of time, the air particles move in all three directions, as follow:

$$(u, v, w) = (U + u', \ V + v', \ W + w') \tag{1}$$

With $u, v, and \ w$ being the total component of the velocity in x (stream-wise), y (lateral), and z (perpendicular to x-y plane) directions. The capital letters $U, V, and \ W$ denote the mean components of the velocity, while u', v', w' are the fluctuations about the mean. For the sake of consistency and to avoid any confusions, these notations have been followed closely throughout the current study.
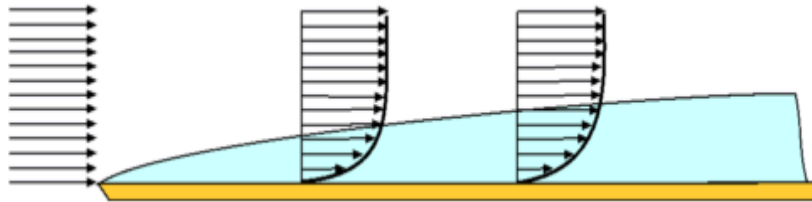

Figure 4: Boundary layer development on a flat plat

As a result of the velocity gradient between the layers of flow, $\frac{du}{dy}$, the shear stress τ develops in the boundary layer. It is this shear stress that causes drag on immersed objects in the fluids.

The boundary layer is thinner over smooth surfaces (sea, ocean or ice) and much thicker over rough surfaces such as hilly, forested or urban terrains with buildings. Inside the boundary layer, the flow is dominated by surface friction and viscous effects. The wind velocity at the surface is zero due to the no-slip condition. The vertical exchange of momentum and heat are

related to the stability of the atmosphere. The stability of the atmosphere indicates whether the atmosphere develops turbulence or waves of growing amplitudes.

The stable stratification happens when the underlying surface is colder than the air, and hence the flow becomes laminar. Under this condition, a weak turbulence is generated by shear and destroyed by viscosity and buoyancy forces.

The unstable condition happens when the underlying surface is hotter than the surrounding air. This causes a vertical movement of air. In unstable conditions, due to the mixing from thermally generated eddies, the turbulent mixing happens at different layers of atmosphere.

At near neutral stability condition, we only have the mechanically generated turbulence which is mainly due to the surface drag.

The vertical variation of mean wind speed, also known as the wind speed profile or wind shear, is modeled using log law or power law. Equation 2, shows the logarithmic law under neutral stability condition as it is the case for wind tunnel testing. In this equation, y_0 is the roughness length (m) associated with the type of terrain, z is the height above the surface, k is the Von-Karman constant which is 2.5, and u_* is the frictional velocity specific to each terrain.

$$U(y) = \frac{u_*}{k} \ln\left(\frac{y}{y_0}\right) \tag{2}$$

The roughness height y_0 can be estimated using Charnock's equation:

$$y_0(U) = \frac{Cu_*^2}{g} = \frac{C}{g} \left[\frac{0.4U}{\ln\left(\frac{y_{hub}}{y_0(U)}\right)}\right] \tag{3}$$

Where C is a constant coefficient between 0.011 for open sea and 0.034 for near coastal regions, g is the acceleration due to gravity. The value of y_0 is small and ranges between 0.001-0.003m for ocean surfaces.

no.	class name	Roughness length: m	landscape features
1	sea	0.0002	open water, tidal flat, snow with fetch above 3 km
2	smooth	0.005	featureless land, ice
3	open	0.03	flat terrain with grass or very low vegetation, airport runway
4	roughly open	0.10	cultivated area, low crops, obstacles of height H separated by at least 20 H
5	rough	0.25	open landscape, scattered shelter belts, obstacles separated by 15 H or so
6	very rough	0.5	landscape with bushes, young dense forest etc. separated by 10 H or so
7	closed	1.0	open spaces comparable with H, e.g. mature forest, low-rise built-up area
8	chaotic	over 2.0	irregular distribution of large elements, e.g. city center, large forest with clearings

Figure 5: Terrain classification and corresponding roughness length (Wieringa, 1992)

The power law is just another method used for modeling vertical variation of mean wind speed. Although, this model is mostly used in wind engineering applications, but there is not any theoretical basis associated with it. In equation 4, y_{ref} is the reference length (m) which is normally the hub height of the turbine, y is the height above the surface, U_{ref} is the wind speed associated with the reference height, and U is targeted velocity at height y, and α is what defines the shape of profile. The value of α would be different for different kinds of terrains.

$$\frac{U}{U_{ref}} = \left(\frac{y}{y_{ref}}\right)^{\alpha} \tag{4}$$

Turbulence intensity is another important parameter used when studying wind, which defines the magnitude of the wind fluctuations. The turbulence intensity, $I_u(y)$, for the longitudinal wind fluctuation, $u(y)$, is defined as:

$$I_u(y) = \frac{\sigma_u}{U(y)} \tag{5}$$

Where $\sigma_u(y)$ is the root mean square of $u(y)$.

Offshore turbulence intensity can be determined using:

$$I_u(y) = \frac{1}{\ln\left(\frac{y_{hub}}{y_0(U)}\right)} + \frac{1.28(1.44 I_{15})}{U} \tag{6}$$

Where I_{15}, is the reference turbulence intensity calculated using the wind speed of 15 m/s, if the exact value is not specified, and 1.28 is the factor corresponding to the 90% quantile value of the turbulence intensity.

At lower altitudes, the turbulence intensity varies with height. Typically, longitudinal turbulence intensity decreases with increasing height near the ground, but it is almost constant at higher elevations above ground. Longitudinal turbulence intensity also decreases with increasing wind speed for the onshore cases. However, for offshore scenario, this is the opposite. For offshore cases, as shown in Figure 6, the turbulence intensity tends to increase with increasing wind speed. This is mainly due to the coupled relationship between the wind speed and the generated waves and currents, as these increase the roughness height.
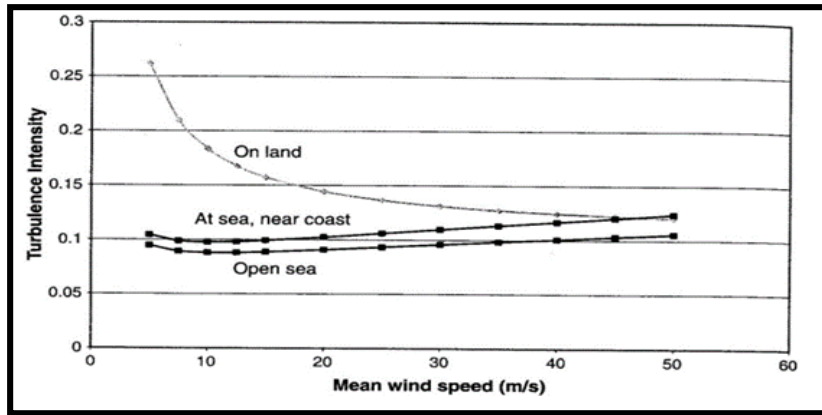

Figure 6: Comparison between the onshore and offshore turbulence intensity

1.3 Literature Review

The wake of a wind turbine is very complex and unsteady in nature. It contains many phenomenon such as tip vortices, vortex shedding, and the shear layer which influence the wake pattern and contribute to the unsteadiness of the flow in the wake.

In a wind farm, because the first row of turbines extract most of the energy from the incoming flow, hence the wake would become more turbulent, and contain lesser amount of energy when compared to the undisturbed incoming flow. The deficit velocity in the wake results in lower energy extraction by the downstream turbines. The increased turbulence in the wake of the turbines would increase the fatigue loading on the downstream turbines, resulting in lowering their lifetime. The study of the wake of the turbines are important and necessary so as to reduce the losses of energy extraction and reducing the fatigue loads on the downstream turbines.

The wake of a wind turbine is divided into near and far wake. The near wake refers to the region approximately one rotor diameter downstream of the turbine. In the near wake, the rotor characteristics such as the number of blades, blade aerodynamics such as stall or attached flows, tip vortices, etc are present. The helical vortices induced by the rotating blades are another important parameter of the near wake. The evolution of helical vortices is responsible for the behavior of the turbulent wake flow structures behind the wind turbines. The tip vortices are an important contributor to noise generation and blade vibration (Massouh and Dobrev 2007). The far wake is the region behind the near wake, where the actual rotor shape is less important, but the focus is on wake modeling, wake interference in wind farms, turbulence modeling, and topographic effects (Vermeer et al 2003).

Many studies have been done to understand the effects of the ambient turbulence intensity on the loading, performance, and wake patterns of horizontal axis wind turbines. Power losses due to the wake effects can reach up to 23% depending on the spacing and alignment of wind turbines (Barthelmie et al., 2009). Field measurements at Horns-Rev offshore wind farm revealed nearly 20% recovery on the maximum power deficit of the downstream turbines at higher ambient turbulence levels (Hansen et al., 2012). Barthelmie & Jensen (2010) also estimated that wind farm efficiency at Nysted wind farm will improve up to 9% in unstable conditions with higher ambient turbulence levels.

In a wind tunnel study performed by Ozbay et al (2012), an increase of 6% was reported in the power output of an onshore wind farm over a similar layout corresponding to offshore scenario and concluded that the higher ambient turbulence intensity is the sole responsible for such phenomena. The analysis done by Chamorro and Porte-Agel (2009) shows strong dependence between the velocity deficit and the atmospheric turbulence.

There is a strong connection between the tip vortex breakdown and the shear layer expansion. Lignarolo et al. (2013) showed that tip-vortices could act against the turbulent mixing; however, the break-down of these vortices could enhance turbulent mixing.
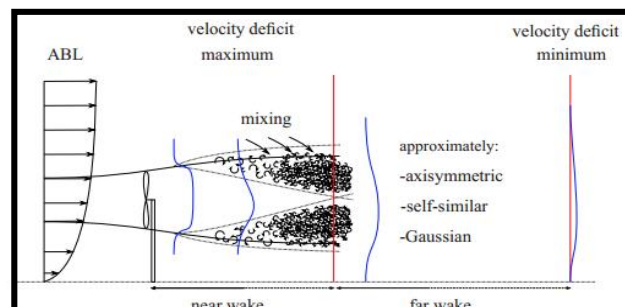

Figure 7: Wake evolution behind a horizontal axis wind turbine
(Sanderse, 2009)

Deep-water offshore environments are characterized by strong wind speeds (due to shallower boundary layer profiles), and lower turbulence intensities (due to smoother surface roughness of offshore environments). Generally, the higher and steadier wind speeds would result in higher energy production. The reduced ambient turbulence of offshore environment will help in reducing the fatigue loads on wind turbine components. But, reduced ambient turbulence will also reduce the entrainment of the turbulent kinetic energy (T.K.E.) from the high energy flow above, and therefore, it causes the wake to travel longer. Hence, the spacing between the offshore turbines may need to be larger in comparison to that of onshore wind turbines.

Rockel et al. (2014) performed a wind tunnel experiment to observe the influence of the platform pitch on the wake of a wind turbine. His results indicated that the platform pitch creates an upward shift in all components of the flow and their fluctuations. He concluded that the vertical flow created by the pitch motion as well as the reduced entrainment of kinetic energy from undisturbed flow above the turbine result in potentially higher loads and less available kinetic energy for a downwind turbine.

Sebastian et al. (2013) performed series of numerical simulations on floating wind turbines, and determined that the blade element momentum theory does not capture the unsteadiness generated in the flow due to significant changes in the angle of attack. Large angle of attack changes were due to the additional motion of the floating platforms. Motion induced unsteadiness violates assumptions of standard blade element momentum theory and leads to inaccurate predictions of unsteady aerodynamic loads. He showed that pitching motion of the wind turbine causes the turbine to change from the windmill state to the propeller state.

1.4 Motivations for the Current Study

Studying the wake of the wind turbines is not a new topic. The wake of wind turbines provide useful information in regards to design optimization of wind turbine's rotors, and help with the lay-out optimization of wind farms. However, most of these studies have been performed on the classical bottom-fixed turbines, as is the case for onshore wind farms. But as we are starting to saturate the suitable areas needed for onshore wind farm developments, there is an urge for going offshore for tapping some of the stronger and steadier winds offshore.

Although, there is a strong public resistance in the U.S. for going offshore for the purpose of wind energy extraction, but installing wind turbines at offshore locations is not a new phenomenon. Installing wind turbines in the waters have been going on for the past two decades in Europe. However, all of these wind turbines have been installed in shallow waters, where the turbines are fixed to the seafloor. Hence, any wake study of such turbines is essentially similar to the wake of onshore wind turbines, with the exception of the interaction between the wake and the changing roughness height, which would be the result of the coupled behavior between the wind speed and the wave dynamics.

However, in deep waters, the turbines would need to be floated. There are many advantages associated with installing wind turbines in deep waters. Deep water offshore environment is characterized by higher wind speed and lower ambient turbulence, which could be very beneficial in terms of increased power extraction, and lowering the fatigue loads on floating offshore wind turbines. However, there are also significant technological challenges associated with floating wind turbines. The dynamic excitation of wind and waves will induce excessive motions along each of the 6 degrees of freedom (6-DOF) of

the floating platforms. These motions will then be transferred to the turbine, and directly impact the turbines' performance, loading and consequently, the wake characteristics of the floating wind turbines.

The effect of the floating motions on offshore wind turbine aerodynamics can be thought, as a stationary turbine operating in a highly unsteady and fluctuating flow. Therefore, it is anticipated that these motions would have significant influence on the entrainment of the T.K.E. in the wake, affecting the distance required between the offshore wind turbines, loading and the power extraction of the downstream turbines.

The motions associated with these floating wind turbines would also increase the mechanically generated turbulence in the wake of these floating turbines, affecting the performance, and the loading on the downstream turbines.

The current experimental research analyzes the wake behavior of a wind turbine subjected to uncoupled base motions (surge, pitch, and heave). Advanced diagnostic technique methods were employed in order to elucidate the underlying physics of a wind turbine subjected to base motions. In the absence of a combined wind-wave basin, and in order to replicate the dynamics of floating offshore wind turbines (FOWT), a 1:300 scaled model wind turbine was installed on a high precision 3-DOF motion simulator device in a well-controlled, closed loop, dry-boundary layer wind tunnel. The inflow conditions of the wind tunnel were matched to the corresponding deep-water offshore environment. A numerical simulation study on an actuator disk was also performed to predict the loading and the performance of a turbine subjected to base motions.

1.5 Thesis Organization

This thesis contains three chapters that are written in thesis format. In chapter 1, a general introduction was given which provided the readers with enough background information and motivation for the current study.

In chapter 2, the experimental set up was explained followed by an in depth information and analysis for surge, pitch and heave motions. At the end of the analysis for each motions, the corresponding plots and contours are presented. Finally in chapter 3, a general conclusion for the current experimental work was provided.

CHAPTER 2

A STUDY OF THE NEAR WAKE CHARACTERISTICS OF A WIND TURBINE MODEL SUBJECTED TO SURGE, PITCH, AND HEAVE MOTIONS

2.1 Introduction

Offshore wind energy is one of the most abundant and promising sources of energy that can provide substantial amount of clean, domestic, and renewable energy. The United States is especially fortunate to be surrounded by vast waters on both sides of the nation. This provides a unique opportunity for offshore wind farm developments in this country. There is over 4000 GW of wind potential within 50 nautical miles of the U.S. coastlines (Musial et al, 2010), which is approximately four times the current U.S. power generation capacity. Offshore wind energy is divided into three categories, depending on the depth of water where the turbines are being installed at. The depth of the water dictates the type of substructure technology needed to install offshore wind turbines. In shallow waters (0 m to 30 m), the turbines are being fixed to the sea floor by means of a monopile or gravity based foundations. In intermediate waters (30m to 60 m), the wind turbines are also being fixed to the sea floor but by different kind of substructures such as jacket or tripods. As the water depth increases beyond 60m, the cost of substructure increases substantially, making it almost economically infeasible to fix the turbines to the sea floor. Therefore, the turbines will need to be floated in deep waters.

By the end of 2014, there were 74 offshore wind farms operating in 11 European countries, yielding over 8 GW of electricity. All of these wind farms are located in shallow waters with depths less than 20 meters where the turbines are fixed to the sea floor (Corbetta G., 2015). Unlike the shallow European waters, the U.S. waters are, on the other

hand, mostly deep with the exception of a few regions in the East Coast and the Gulf of Mexico. Therefore, offshore wind farm development in the U.S. will most likely be based on the floating concept.

There are many advantages of floating wind turbines in deep waters, however, there are also significant technological challenges associated with it too. There are six degrees of freedom (6-DOF) associated with any floating structures, three displacements (surge, sway, and heave) and three rotations (roll, pitch, and yaw). The dynamic excitation of wind and waves, will induce excessive motions along each of the 6-DOF's of the floating platform. These motions will then be transferred to the turbine itself, and directly impact the turbines' performance, and loadings.

The most common types of floating platforms that have been proposed for wind turbine applications include; semi-submersible, tension leg platform, and spar buoy. However, regardless of the type, floating platforms cannot easily provide high degrees of stability for mounting wind turbines. This is especially true for the Horizontal Axis Wind Turbines (HAWT). For a HAWT system, the mass of the floater is of the same order of magnitude as the mass of the nacelle and rotor assembly, and therefore, the center of gravity (C.G.) of a HAWT system would be located at a much higher location in relation to their Center of Buoyancy (C.B.), hence, creating an unstable floating structure. Therefore, any external forces seen by the floater, will influence the rotor assembly, and any forces felt by the rotor assembly will be affecting the floater system.

The study of both coupled and uncoupled motions of the floating turbines are important and necessary to determine the contributions of each motions along each of the DOFs to the overall performance, and the wake characteristics of floating wind turbines. However, the current study investigates the effects of uncoupled surge, pitch, and heave motions, on

the performance, loading, and the wake characteristics of the turbine. The surge motion is defined as the linear translation of the turbine in stream-wise direction. The heave motion is also defined as the linear translation of the turbine but in vertical direction. However, the pitch motion is the angular motion of the turbine in stream-wise direction. Based on the previous numerical simulation done on a floating offshore wind turbine, all of these motions (surge, pitch, and heave) are believed to be the most dominant motions associated with a floating turbine.

The wake of wind turbines contains many information relevant to design and optimization of wind turbines, and hence important to study. The wake of a wind turbine is divided into near and far wake. The near wake refers to the region approximately one rotor diameter downstream of the turbine. In the near wake, the rotor characteristics such as the number of blades, blade aerodynamics such as stall or attached flows, tip vortices, etc are present. The helical vortices induced by the rotating blades are another important parameter of the near wake. The evolution of helical vortices is responsible for the behavior of the turbulent wake flow structures behind the wind turbines. The tip vortices are an important contributor to noise generation and blade vibration (Massouh and Dobrev 2007). The far wake is the region behind the near wake (any region behind 1 diameter downstream of the rotor), where the actual rotor shape is less important, but the focus is on wake modeling, wake interference in wind farms, turbulence modeling, and topographic effects (Vermeer et al 2003).

Many studies have been done to understand the effects of the ambient turbulence intensity on the loading, performance, and wake patterns of horizontal axis wind turbines. Power losses due to the wake effects can reach up to 23% depending on the spacing and alignment of wind turbines (Barthelmie et al., 2009). Field measurements at Horns-Rev

offshore wind farm revealed nearly 20% recovery on the maximum power deficit of the downstream turbines at higher ambient turbulence levels (Hansen et al., 2012). Barthelmie & Jensen (2010) also estimated that wind farm efficiency at Nysted wind farm will improve up to 9% in unstable conditions with higher ambient turbulence levels.

In a wind tunnel study performed by Ozbay et al (2012), an increase of 6% was reported in the power output of an onshore wind farm over a similar layout corresponding to offshore scenario and concluded that the higher ambient turbulence intensity is solely responsible for such phenomena. The analysis done by Chamorro and Porte-Agel (2010) shows strong dependence between the velocity deficit and the atmospheric turbulence.

Rockel et al. (2014) performed a wind tunnel experiment to observe the influence of the platform pitch on the wake of a wind turbine. His results indicated that the platform pitch creates an upward shift in all components of the flow and their fluctuations. He concluded that the vertical flow created by the pitch motion as well as the reduced entrainment of kinetic energy from undisturbed flow above the turbine result in potentially higher loads and less available kinetic energy for a downwind turbine.

Sebastian et al. (2013) performed series of numerical simulations on floating wind turbines, and determined that the blade element momentum theory (BEM) does not capture the unsteadiness generated in the flow due to significant changes in the angle of attack. Large angle of attack changes were due to the additional motion of the floating platforms. Motion induced unsteadiness violates assumptions of standard blade element momentum theory and leads to inaccurate predictions of unsteady aerodynamic loads. He showed that pitching motion of the wind turbine causes the turbine to change from the windmill state to the propeller state.

A set of comprehensive experimental studies were performed to analyze the near wake characteristics of a wind turbine subjected to uncouple base motions: surge, heave, and pitch. Furthermore, a numerical simulation based on the 2-D actuator disk theory was also performed to analyze the loading and the performance of a disk subjected to uncoupled motions: surge, heave, and pitch. In order to better understand the underlying physics of the oscillating turbine, the results were then compared to a traditional bottom fixed turbine.

2.2 Experimental Setup

The present experimental study is performed in the large-scale Aerodynamic/Atmospheric Boundary Layer (AABL) wind and gust tunnel located in the Department of Aerospace Engineering at Iowa State University. The AABL wind tunnel is a closed-circuit wind tunnel with a boundary-layer test section 20 m long, 2.4 m wide and 2.3 m high, optically transparent side walls, and with a capacity of generating a maximum wind speed of 40 m/s in the test section. Arrays of chains were laid-out on the wind tunnel's floor on the upstream side of the wind turbine model in order to match the flow to that of offshore environment. The boundary layer growth of the simulated ABL wind under almost zero pressure gradient condition was achieved by adjusting the ceiling height of the test section of the wind tunnel. The oncoming boundary layer wind velocity profile was fitted by using Equation 1, where y_{ref} is a reference height (hub) and U_{ref} is the wind speed at the reference height. The power law exponent 'α' is associated with the local terrain roughness. Figure 1, shows the measured stream-wise mean velocity (normalized with respect to the hub height velocity, U_{hub}) and the turbulence intensity profiles of the oncoming flow in the test section for the present study. The power law exponent in

Equation 1 was found to be α = 0.10, corresponding to the open sea boundary layer profile according to the Japanese standard (AIJ or Architecture Institute of Japan). GL (Germanischer Lloyd) regulations define a turbulence intensity of 0.12 at the hub height of offshore wind turbines; however, this value was determined to be very conservative compared to field measurements. However, the values of α, and the turbulence intensity for offshore locations are site specific and they can vary greatly depending on whether we are talking about the near coast or open seas. For the current experimental study, a turbulence intensity of 10% at the hub height of the model turbine was chosen.

$$\frac{U}{U_{ref}} = \left(\frac{y}{y_{ref}}\right)^{\alpha} \tag{1}$$
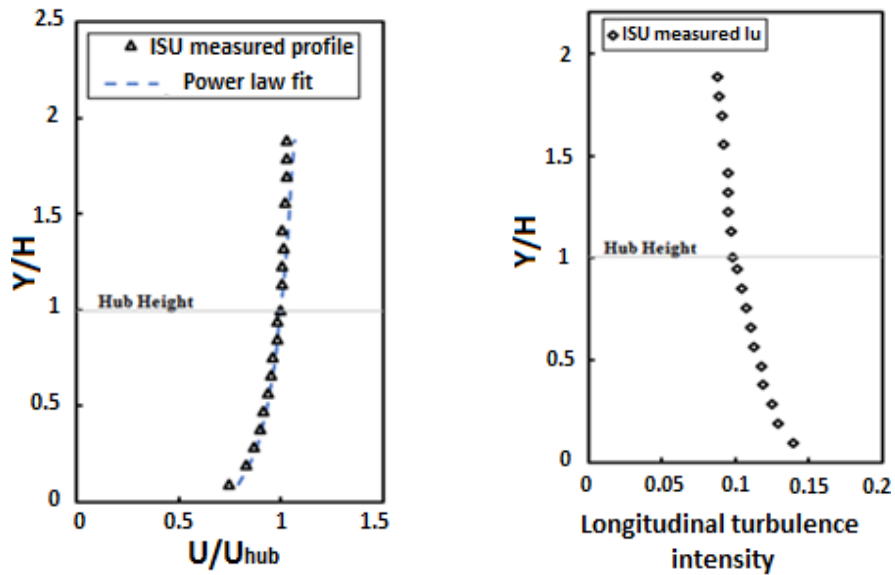
Figure 8: Measured stream-wise wind speed and the longitudinal turbulence intensity profiles

Figure 9 shows, a 1:300 geometrically scaled model horizontal axis wind turbine (HAWT) of height 270 mm (81m in full scale) measured from the wind tunnel's floor to the hub height of the turbine. However, the base of the turbine's tower was extended

beyond the tunnel's floor to connect it to the motion simulator fixed underneath the tunnel (an additional height of 130mm). The rotor diameter for this scaled model was chosen as 300 mm (90m in full scale), and the turbine was developed using rapid prototyping method. The rotor blades were designed based on the ERS-100 prototype turbine blades developed by TPI Composites, Inc. The rotor blade has a constant circular cross section from the blade root to 5% blade radius (R), and three NREL airfoil profiles (S819, S820, S821) were used at different span-wise locations along the rotor blade. The S821 airfoil profile spans between 0.208R and 0.40R, the S819 primary airfoil is positioned at 0.70R, and the S820 airfoil profile is specified at 0.95R. For optimal performance of the rotor, the blades were pitched by 3 degrees.
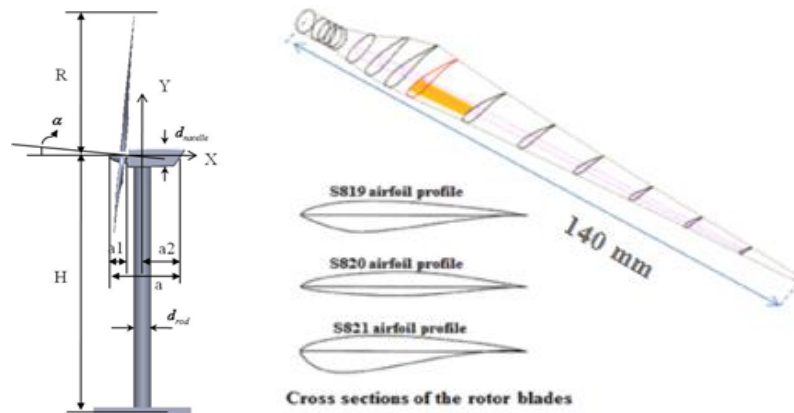
Figure 9: The design parameters of the model wind turbine

The blockage ratio was calculated to be around 1.3%, which is well within the acceptable limit of 5%. The incoming velocity, U_∞, was set as 3.5m/s at the hub height of the turbine that provided a rotational speed of 17 Hz for the model turbine. The Reynolds number corresponding to the prototype wind turbines range between 500,000 to 6,000,000. However, the corresponding diameter based Reynolds number (Re_D) for this experiment

was 71000 which was much lower than that of the large-scale wind turbines operating in the fields.

A tip-speed-ratio (TSR) of 4.5 was maintained throughout the test. The tip-speed-ratio, is the ratio between the rotational velocity of the turbine to the free-stream velocity.

$$TSR = \frac{\Omega R}{U_\infty} \tag{2}$$

where Ω is the angular velocity of the model turbine in rad/s.

Besides matching the TSR between the model and the prototype wind turbines, other scale relationships must also be maintained when dealing with floating wind turbines (Martin et al, 2012).

Froude number is the ratio between the inertial to gravitational forces. Matching Froude scale ($\lambda_{Fr} = 1$), is the method of choice when dealing with hydrodynamic testing of scaled model floating wind turbines.

By using Froude scaling, the wave forces and response of the floater will be correct (ignoring the scale effect in viscous forces). The wind loads on the turbine should also be scaled using Froude scaling, otherwise the floater motions will not be correct. In hydrodynamic testing, this is achieved by calibrating the correct wind forces, rather than the correct wind velocity. Therefore, once the Froude scaling is applied to the wind velocity, further adaptation of wind velocity will be required in order to achieve an acceptable thrust load on the turbine.

However, in wind tunnel model study of offshore wind turbine, the Froude scaling may not be an appropriate similitude method. This is mainly because the wind speed need to be adjusted to obtain the correct wind loads on the turbine, if the range of motions on the scaled model turbine as determined using Froude scaling is to be maintained. Therefore,

matching Froude number would not be able to accurately capture the characteristics of a floating turbine that is subjected to base motions.

A scaling method termed here as velocity ratio method was therefore chosen for the current study in order to capture the important characteristics of the wake of the turbine subjected to surge motions. The velocity ratio method was achieved by maintaining the ratio between the maximum velocity of the surge motion to the freestream velocity for both the model and the prototype.

$$\left(\frac{U_{surge}}{U_\infty}\right)_{prototype} \quad \sim \quad \left(\frac{2Af}{U_\infty}\right)_{model} \tag{5}$$

Where A is the amplitude of displacement and f is the frequency of oscillation in Hz for the surge motion. The motion simulator devices that were used for the current experimental studies included: an M-ILS150cc (for surge), an M-ILS100cc (for heave motion), and an URS50BCC (for pitch) high precision linear and rotation stages motion simulator manufactured by Newport Corporations and was used to replicate the surge, heave, and pitch motions of a floating wind turbine. The motion simulator device was carefully installed under the test section floor of the wind tunnel to avoid any flow disturbances due to the presence of such device. The turbine was then placed on top of the motion simulator through a special cut in the tunnel's floor, to prevent the air from leaking out of the tunnel.

A 2-D Particle Image Velocimetry (PIV) technique was used (as shown in Figure 10) to capture whole-field information of the wake of both the bottom fixed turbine and the turbine with the surge motion. The coordinate system indicating three velocity components is also shown in Figure 10. The flow was seeded with 1-5 μm oil droplets and the laser system used for illumination of the seeding particles was a double-pulsed Nd:YAG laser (Ever Green big sky laser series) emitting two 200 mJ laser pulses at a wavelength of 532

nm and with a repetition rate of 1 Hz. For a better accuracy in results, the laser sheet thickness was adjusted to be around 1 mm. Two high-resolution (2048×2048 pixels) charge-coupled device (CCD) cameras with axis perpendicular to the laser sheet was used for PIV image acquisition. The CCD camera and the double-pulsed Nd:YAG lasers were connected to a workstation via a digital delay generator that controlled the timing of both the laser illumination and the image acquisition.
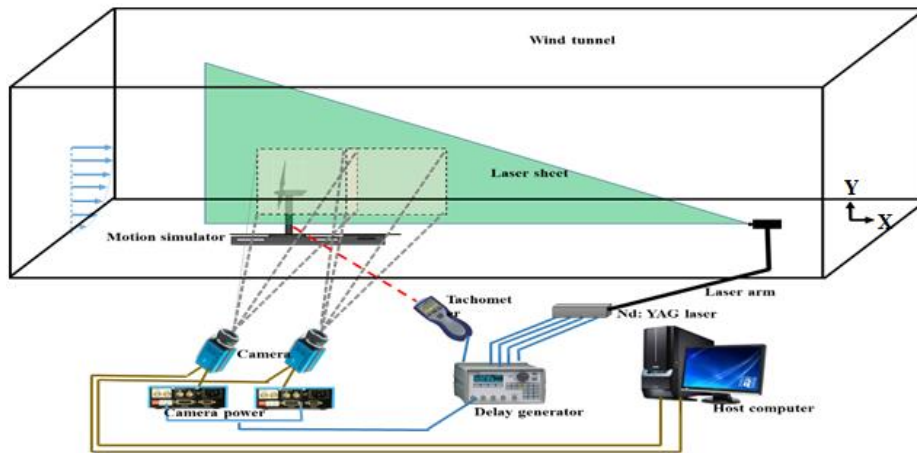
Figure 10: Illustration of the PIV set-up

Instantaneous PIV velocity vectors were obtained using a frame-to-frame cross correlation technique involving successive frames of patterns of particle images in an interrogation window with 32×32 pixels and an effective overlap of 50% to satisfy the Nyquist criterion. The ensemble averaged flow quantities such as mean velocity, turbulent-velocity fluctuations, normalized turbulent kinetic energy, and Reynolds shear stress distributions were obtained from approximately 1000 frames of instantaneous PIV measurements. The measurement uncertainty level for the velocity vectors was estimated to be within 2.0%, and that of the turbulent velocity fluctuations and turbulent kinetics energy was about 5.0%.

As shown in Figure 10, the x-coordinate corresponds to the stream-wise direction with the origin located at the center of the tower of the turbine. The y-coordinate which is in lateral direction, with its origin at the center of the nacelle. Using the right hand rule, the z-coordinate would then be perpendicular to the x-y plane and will be pointing to the right side of the wind tunnel's wall.

2.3 Results and Analysis of the Surge Motion

The flow field (x/D < 1.8) measurements behind a wind turbine subjected to uncoupled surge motion was carried out by using a high-resolution PIV system, and the wake results obtained at particular pitch angles were then compared to those of a classical bottom-fixed turbine.

The surge motion is believed to be the most dominant linear motion associated with a floating offshore wind turbine, and defined as the linear translation of the turbine along the wind direction (in stream-wise direction).

The exact motion for the prototype turbine was determined using the previous numerical simulation results. Using Equation 5, the freestream velocity at the hub height of the scaled model turbine was set to 3.5 m/s, the constant surge velocity was chosen to be $0.1\frac{m}{s}$ with a displacement of $\binom{+}{-}$ 6 cm and therefore, the frequency of oscillation was needed to be around 0.5 Hz. However, due to limitation of the motion simulator, this frequency was kept at 0.2 Hz instead.

As shown in Figure 11, the three critical locations for the current study of the surge motion include; front (6 cm ahead of the neutral location), center (the neutral location), and the back location (6 cm behind the neutral location). The flow measurements were used to quantify the

differences in the wake of the oscillating turbine in surge motion when the aerodynamic hysteresis occurs. In the hysteresis loop, the differences in the wake flow at the same surge condition were examined along the increasing surge location (i.e., the turbine is moving *with the flow*) and the decreasing surge location (i.e., the turbine is moving *into the flow*) branches.
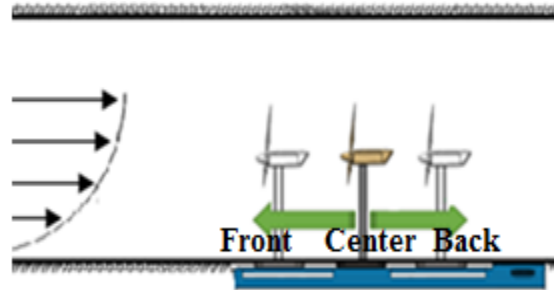
Figure 11: Illustration of turbine's oscillation in surge motion

The measurement plane was composed of two fields with an overlap of 15mm length, and two CCD cameras were used to acquire images from these fields. Two fields were then merged in Tecplot to acquire the image in the measurement plane. Finally, ensemble averaged flow quantities, such as mean flow velocity, Reynolds stresses and Turbulence Kinetic energy, were analyzed.

Figure 12, shows the contour plots accompanied by their extracted data (at x/D = 0.8 and x/D=1.7) of the PIV measurements of the averaged stream-wise velocity (U/Uhub) profiles in the wake of a bottom fixed turbine (a), and the center location for a turbine oscillating in surge motion: as it is moving with the flow (b), as it is moving into the flow (c), and the averaged of the forward and backward motion(d). Each of the contour plots are accompanied by their extracted data (at x/D = 0.8 and x/D=1.7) of the PIV measured normalized stream-wise

velocities. Figure 17 and Figure 20 also provide the same plots corresponding to the front and back locations, respectively.

As can be seen in Figure 12, there is clear evidence of the deficit in the velocity in the wake of both; the bottom fixed turbine and the moving turbine. This deficit is the result of energy extraction by the turbine itself. Double peaks are observed and understood as characteristic of the near wake profiles (X/D <1). But as we go farther down in the wake (X/D >1), the double peaks die out and become just a single peak. This single peak eventually dies out in approximately 15~20 diameter downstream of the turbine, where the flow gains its fullest momentum and becomes the undisturbed flow again. There is some overshoot at the top region of the profiles in the near wake regions, corresponding to the plots of both turbines which suggests that the flow is accelerating at near top-tip of the blade, and also could be an evidence of the blockage effect caused by the existence of the turbine itself.

From the extracted data of Figure 12b and 12c, during the surge motion, as the turbine is at the center location and is moving with the flow (to the right), it's wake tends to accelerate when compared to the wake of the bottom fixed turbine, suggesting a reduced energy extraction by the rotor. This trend is anticipated to become more pronounced as we go down farther in the wake. However, as the turbine is moving into the flow (to the left), the wake of the turbine in surge motion becomes very similar to the wake of the bottom-fixed turbine. Therefore, with the current prescribed range of motions, the current surge velocity, and the frequency, there would be no significant difference between the power extraction by the turbine in surge motion at the center location and the bottom-fixed turbine (see Figure 12d).

Figure 13, presents the contours of the normalized lateral component of the velocity (V/Uhub) for both the bottom fixed turbine and the oscillating turbine moving with the flow and into the flow. From the contour plots it is clearly evident that the motion of the turbine

greatly influences the vertical movements of the flow in the wake of the turbine. As the turbine is moving into the flow, it generates a higher rate of vertical motion in the wake when compared to the bottom fixed turbine. However, as the turbine is moving with the flow, it generates lesser amount of motion in vertical direction, when compared to the bottom fixed turbine. Averaging the motions, would also show an increased amount in the lateral movement of the flow, when compared to the results of the bottom fixed turbine.

Figure 14, shows the Reynolds shear stress ($\tau = \frac{-u'v'}{U_{hub}^2}$) and momentum flux ($\frac{\frac{\partial U}{\partial Y}*Ruv*D}{U_{hub}^3}$) plots. The Reynolds shear stress deals with the transport of momentum from high energy flow above the rotor to the lower energy area of the wake region. The momentum flux which is the rate of change of momentum is also another indicator on how fast the higher energy flow above the turbine is being fed into the lower energy area of the wake region. Therefore, both the Reynolds shear stress and momentum flux are directly related on how fast the wake is recovering.

The momentum flux observed in the top tip (shear) layer of the oscillating turbine, and the areas covered by negative fluxes and the magnitudes of these fluxes were found to increase slowly as the wake flow advects downstream for the floating turbine. The negative valued momentum fluxes could be used as an indicator of the flow into the wake centerline. Therefore, the high momentum flow above the shear layer could mix with the wake flow characterized with greater velocity deficits. The expansion of the top tip shear region towards the wake centerline was also observed in Figure 7 as a result of strong mixing. These momentum fluxes could play a significant role in wind farms having clusters of wind turbines by accelerating the wake recovery in the far wake region. As a result, downstream turbines could extract more energy from the disturbed flow. As can be clearly seen in the Reynolds shear stress plots in Figure 14, as the turbine is moving into the flow, it generates substantially higher Reynolds

shear stress in comparsion to the bottom fixed turbine. However, the amount of Reynolds shear stress generation is much lower for the case when the turbine is moving with the flow in comparison to the bottom fixed turbine. However, averaging the motions of both directions would show slight decrease in the amount of momentum transport from the higher energy flow into the wake region.

Figure 15, shows the turbulent kinetic energy ($T.K.E. = \frac{1}{2}\frac{[u'^2+v'^2]}{U_{hub}^2}$). T.K.E. is the kinetic energy per unit mass associated with the eddies in the turbulent flows. T.K.E. deals with the diffusivity effect which is responsible for enhanced mixing. By studying T.K.E., one can determine on how fast the wake is recovering. The fluctuating components of the oncoming boundary layer flow influences the turbulent wake flow structure significantly. For a uniform flow, mean shear distribution in the turbine wake could be axisymmetric with strong shear layer (associated with TKE production) at the levels of bottom-tip and top-tip. However, for an oncoming boundary layer flow with non-uniform mean flow velocity distribution, previous experimental and numerical studies showed that maximum TKE production would occur at the top-tip level as a result of strong shear-produced turbulence and turbulent fluxes (Hu et al., 2012; Zhang et al., 2012; Porte-Agel et al., 2011; Wu et al., 2012). Turbulent fluxes produced due to wake induced turbulence were found to play an important role on the entrainment of energy from the flow above the wind farm (Meyers and Meneveau, 2013). As can be seen in Figure 15, the T.K.E. production increases substantially when the turbine is moving into the flow compared to the bottom fixed turbine. However, as the turbine is moving with the flow, this amount is much lower than the bottom fixed turbine.

Figure 16, show the normalized phase-locked ($\frac{w_z D}{U_{hub}}$) vorticity distributions in the wake of the bottom fixed turbine and the turbine oscillating in surge motion at a phase angle of $\theta = 0°$.

The vorticity (w_z) values were derived from the phase locked velocity distributions in the streamwise and vertical directions by using the expression $w_z = \frac{dV}{dx} - \frac{dU}{dy}$. The phase-locked PIV measurements could be used to identify the unsteady vortex structures (i.e., tip and root vortices, and vortices formed within the nacelle boundary layer) generated in the wake.

As shown in Figure 16, the tip vortices were formed in the strong shear layer located at the uppermost level of the wake. Interestingly, an additional array of concentrated vortices were found to shed from the inboard section located at approximately 50% - 60% of the blade span. The origin of these secondary vortices could be attributed to the desgin imperfection of the blades, which resulted in a seperation in the flow and hence generating vortices. Furthermore, these vortex structures were found to expand outwards as they convect downstream and finally merge with those shedding from the blade tips. Moreover, these additional array of concentrated vortices were found to be larger and stronger than those generated by the blade tips. The vortices formed within the nacelle boundary layer with those shedding from the blade root section were found to dissipate much faster than those generated at the tip and inboard section of the blade.

There is a strong connection between the tip vortex breakdown and the shear layer expansion. Lignarolo et al. (2013) showed that tip-vortices could act against the turbulent mixing; however, the break-down of these vortices could enhance turbulent mixing.

The effect of the hysteresis loop on the evolution (i.e., formation, shedding and dissipation) of the unsteady vortex structures for the bottom fixed turbine and the oscillating turbine are shown in Figure 16. The hysteresis loop was found to make no significant changes on the evolution of the unsteady vortex structures. However, slight changes in the shape and magnitude of the vortex structures can be seen. Furthermore, contrary to the bottom fixed

turbine, the vortex shedding from the inboard and tip sections of the turbine blade were found to break-down/dissipate faster for the oscillating turbine. However, the behavior of the vortex shedding from the nacelle boundary layer and blade root section was pretty similar for the fixed and the turbine in surge motion.
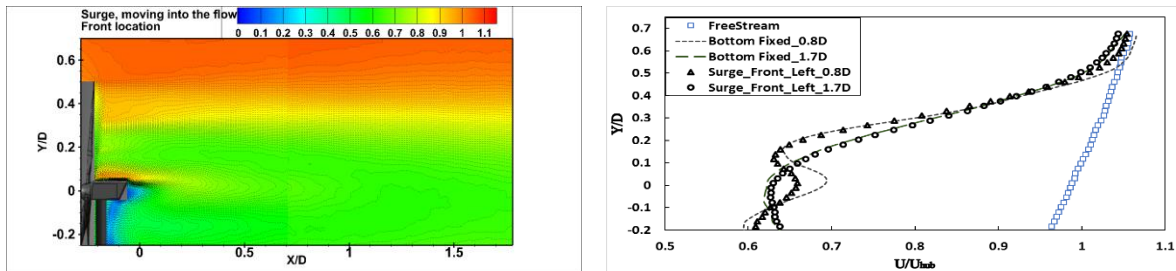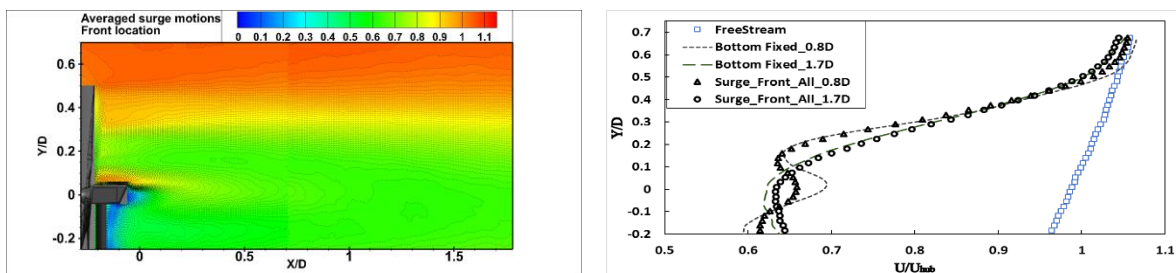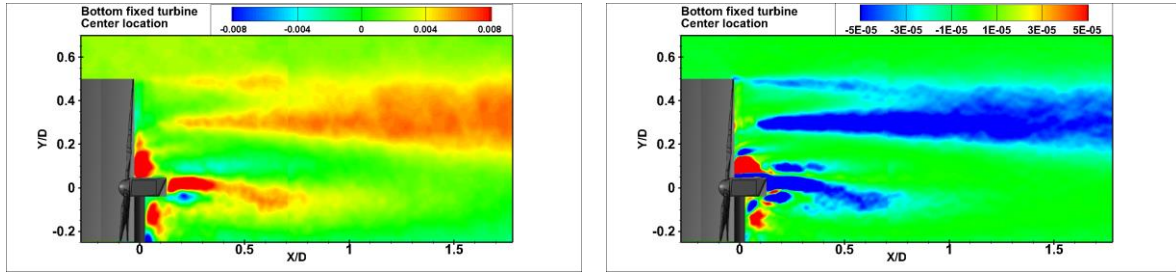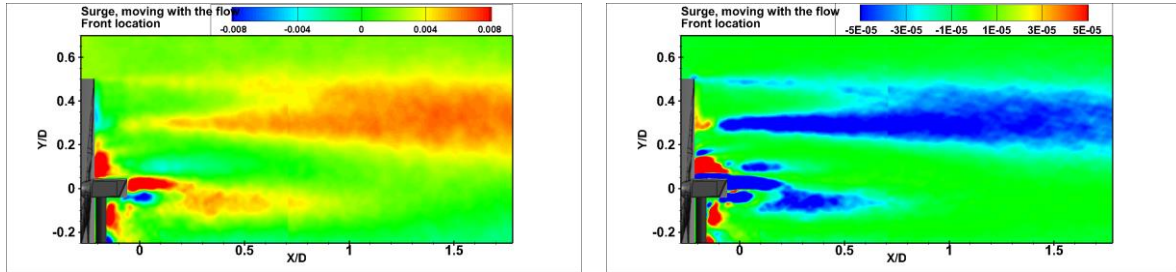
(a) Bottom Fixed Turbine – U/Uhub – Center location

(b) Surge Motion – U/Uhub – Center location – Moving with the flow (→)

(c) Surge Motion – U/Uhub – Center location – Moving into the flow (←)

(d) Surge Motion – U/Uhub – Center location – Averaged Motion
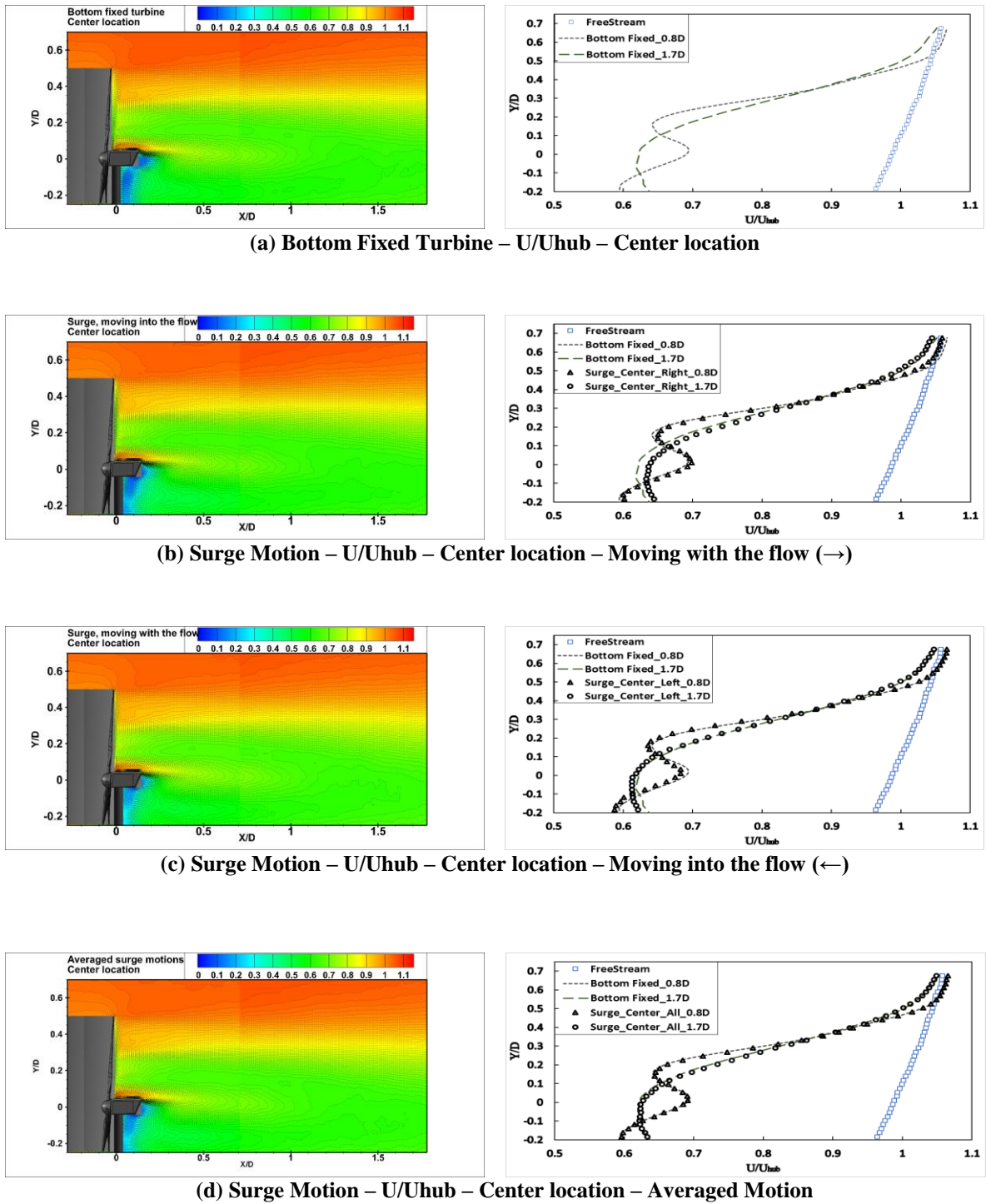
Figure 12: Normalized stream-wise velocity (U/Uhub) profiles in the wake of a bottom fixed turbine (a), and the center location for a turbine oscillating in surge motion: as it is moving with the flow (b), as it is moving into the flow (c), and the average of the forward and backward motion(d).
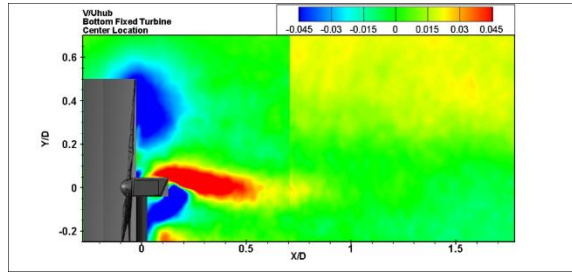
(a) Bottom Fixed Turbine – V/Uhub – Center location
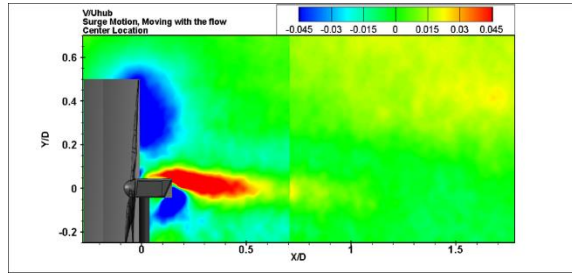
(b) Surge Motion – V/Uhub – Center location – Moving with the flow (→)
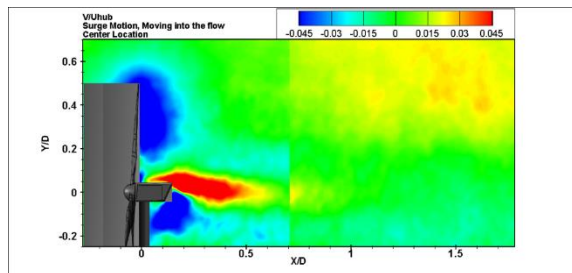
(c) Surge Motion – V/Uhub – Center location – Moving into the flow (←)
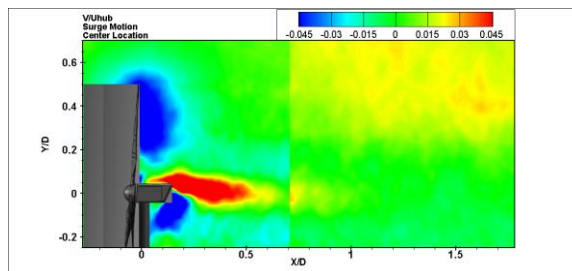
(d) Surge Motion – V/Uhub – Center location – Averaged Motion

Figure 13: Normalized lateral velocity (V/Uhub) profiles in the wake of a bottom fixed turbine (a), and the center location for a turbine oscillating in surge motion: as it is moving with the flow (b), as it is moving into the flow (c), and the average of the forward and backward motions (d).
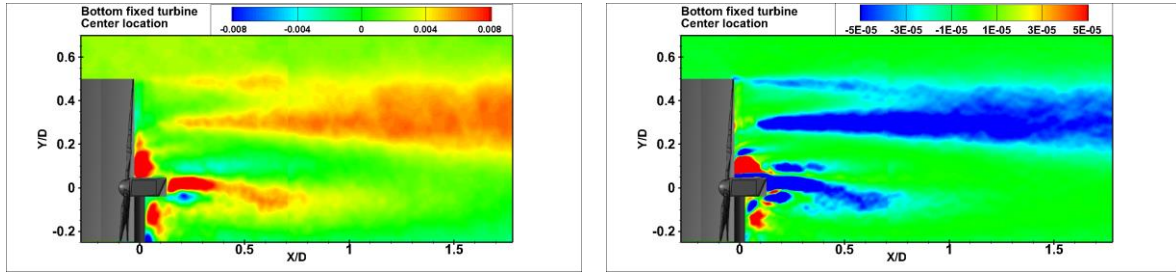
(a) Bottom Fixed Turbine – Reynolds Shear Stress and Momentum Flux – Center location
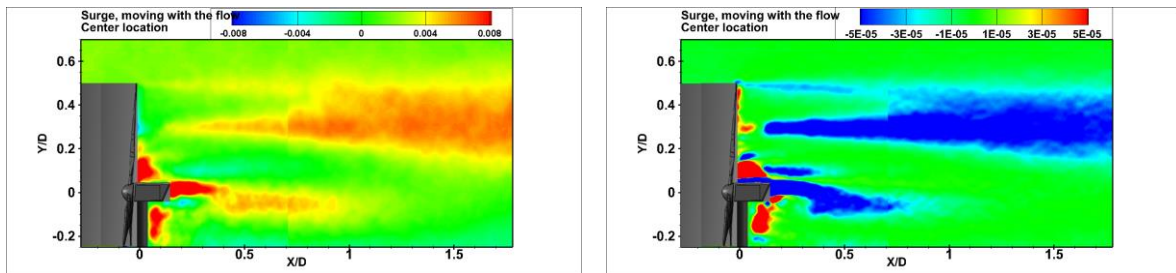
(b) Surge Motion–Reynolds Shear Stress and Momentum Flux–Center location–Moving with the flow (→)

(c) Surge Motion – Reynolds Shear Stress and Momentum Flux – Center location – Moving into the flow (←)

**(d) Surge Motion – Reynolds Shear Stress and Momentum Flux – Center location – Averaged Motion**

Figure 14: Normalized Reynolds Shear Stress $(\frac{Ruv}{U_{hub}^2})$ and the Momentum Flux $(\frac{\frac{\partial U}{\partial Y}*Ruv*D}{U_{hub}^3})$ plots in the wake of a bottom fixed turbine (a), and the center location for a turbine oscillating in surge motion: as it is moving with the flow (b), as it is moving into the flow (c), and the average of the forward and backward motions (d).
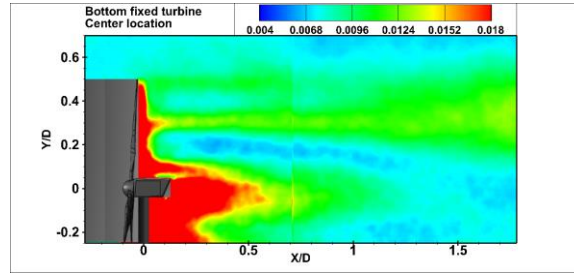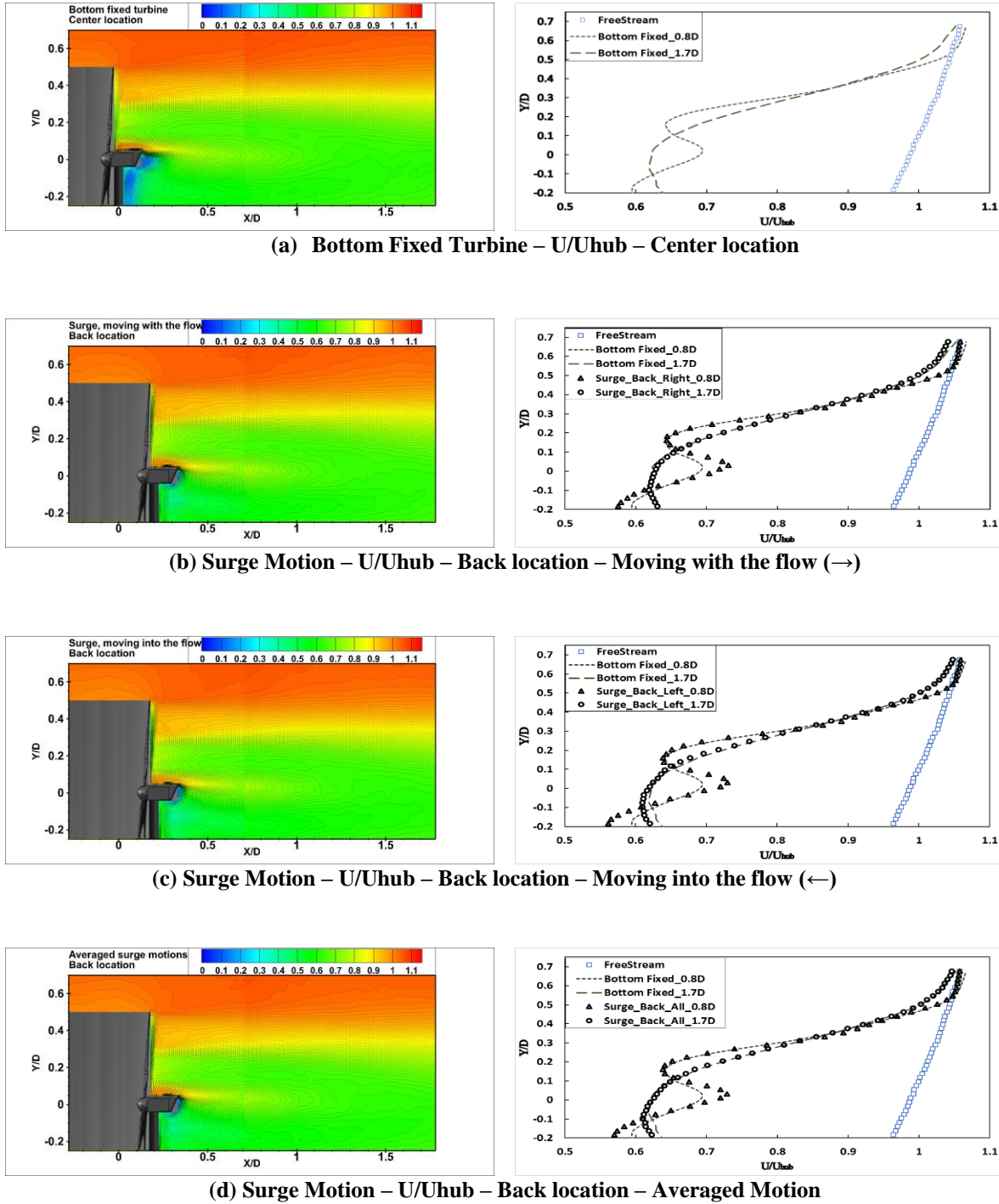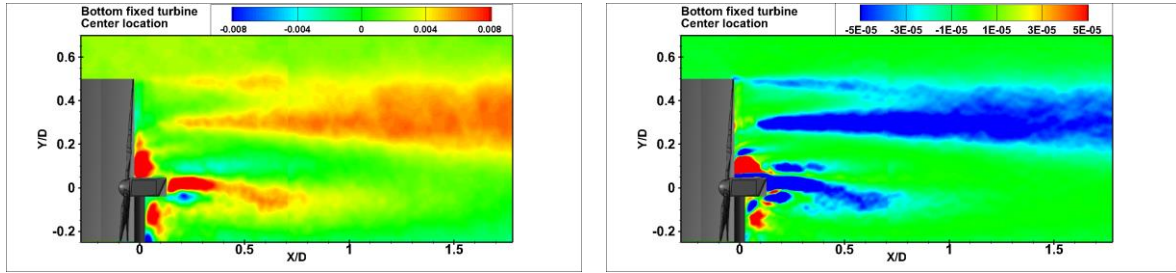
(a) Bottom Fixed Turbine – Center location – T.K.E.
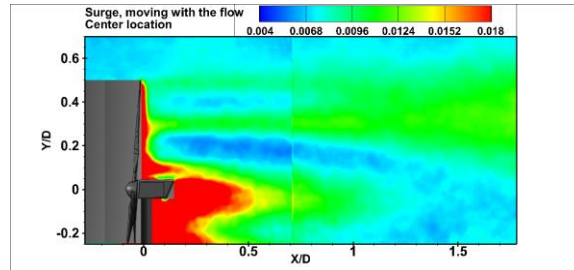
(b) Surge Motion – Center location – Moving with the flow (→) – T.K.E.
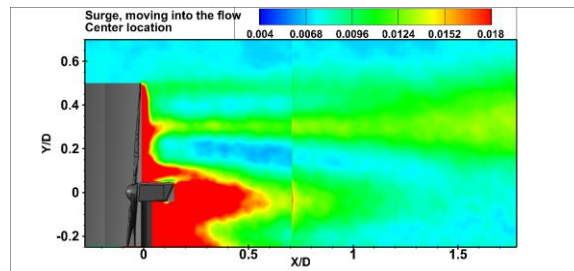
(c) Surge Motion – Center location – Moving into the flow (←) – T.K.E.
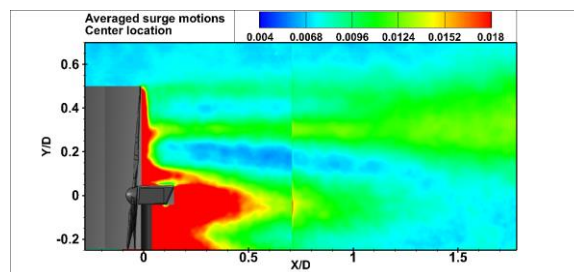
(d) Surge Motion – Center location – Averaged Motion – T.K.E.

Figure 15: Normalized Turbulent Kinetic Energy $(\frac{T.K.E.}{U_{hub}^2})$ plots in the wake of a bottom fixed turbine (a), and the center location for a turbine moving in surge motion: as it is moving with the flow (b), as it is moving into the flow (c), and the averaged forward and backward motions (d).
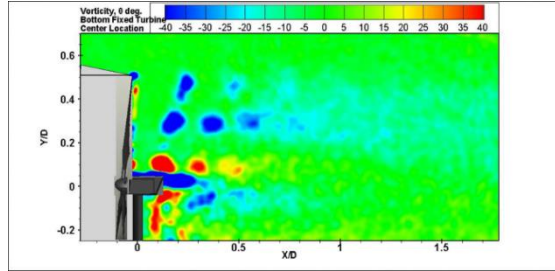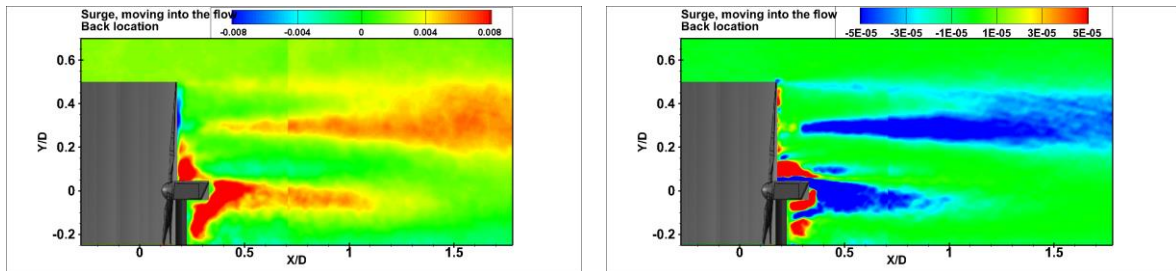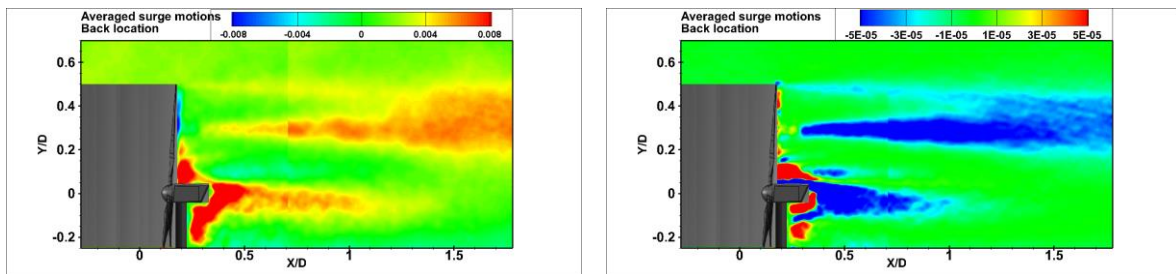
(a) Bottom fixed turbine – Vorticity – Center location
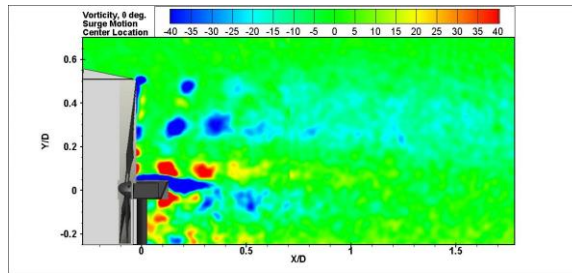
(b) Surge motion – Averaged Motion – Vorticity – Center location (→)
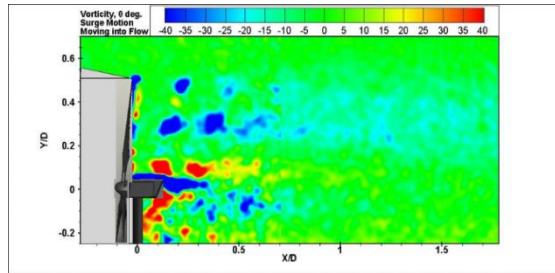
(c) Surge Motion – Moving into the flow – Vorticity – Center location (←)
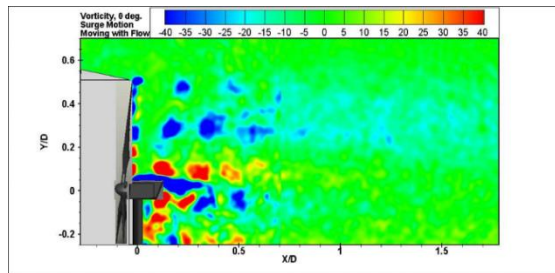
(d) Surge motion – Moving with the flow – Vorticity – Center location

Figure 16: Normalized vorticity distribution $(\frac{w_z D}{U_{hub}})$ plots in the wake of a bottom fixed turbine (a), and the center location for a turbine moving in surge motion: the averaged forward and backward motions(b), as it is moving with the flow (c), as it is moving into the flow (d).
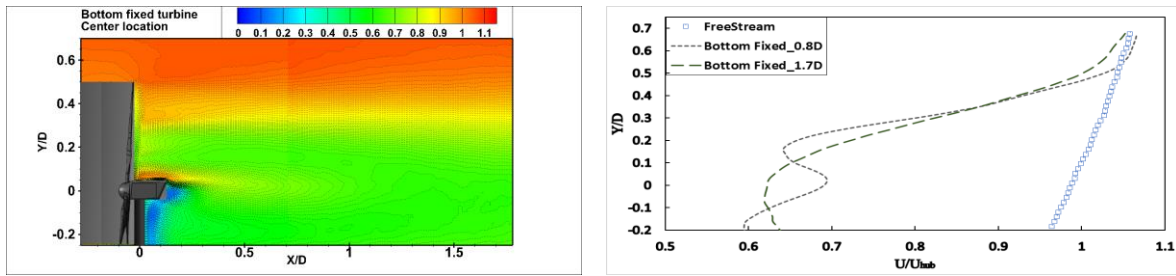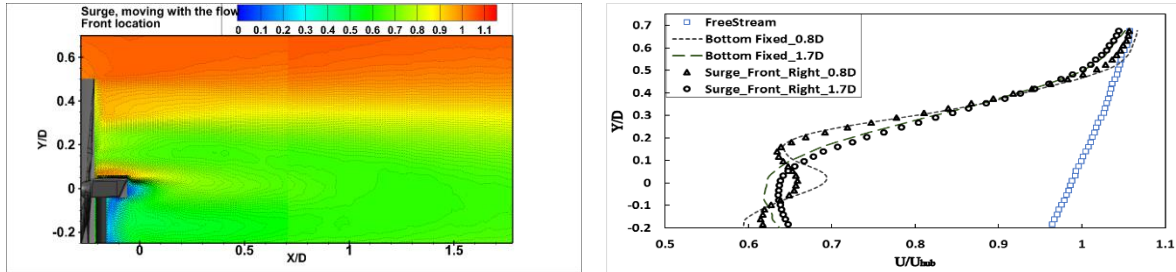
(a) **Bottom Fixed Turbine – U/Uhub – Center location**

(b) **Surge Motion – U/Uhub – Front location – Moving with the flow (→)**

(c) **Surge Motion – U/Uhub – Front location – Moving into the flow (←)**

(d) **Surge Motion – U/Uhub – Front location – Averaged Motion**

Figure 17: Normalized stream-wise velocity (U/Uhub) profiles in the wake of a bottom fixed turbine (a), and the Front location for a turbine oscillating in surge motion: as it is moving with the flow (b), as it is moving into the flow (c), and the average of the forward and backward motion(d).

(a) Bottom Fixed Turbine – Reynolds Shear Stress and Momentum Flux – Center location

(b) Surge Motion–Reynolds Shear Stress and Momentum Flux–Front location–Moving with the flow (→)

(c) Surge Motion – Reynolds Shear Stress and Momentum Flux – Front location – Moving into the flow (←)

(d) Surge Motion – Reynolds Shear Stress and Momentum Flux – Front location – Averaged Motion

Figure 18: Normalized Reynolds Shear Stress ($\frac{Ruv}{U_{hub}^2}$) and the Momentum Flux ($\frac{\frac{\partial U}{\partial Y}*Ruv*D}{U_{hub}^3}$) plots in the wake of a bottom fixed turbine (a), and the front location for a turbine oscillating in surge motion: as it is moving with the flow (b), as it is moving into the flow (c), and the average of the forward and backward motions (d).
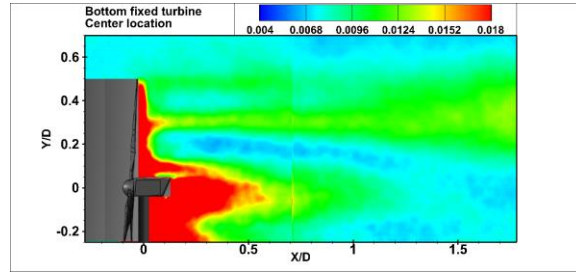
(a) Bottom Fixed Turbine – Center location – T.K.E.
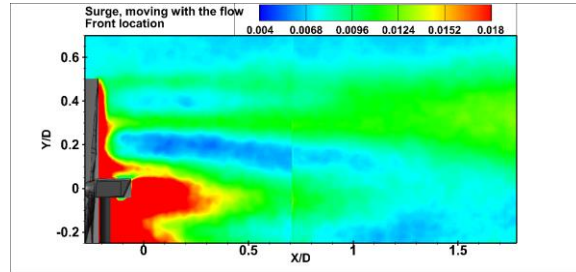
(b) Surge Motion – Front location – Moving with the flow (→) – T.K.E.
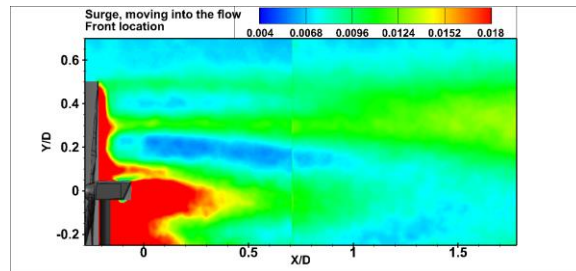
(c) Surge Motion – Front location – Moving into the flow (←) – T.K.E.
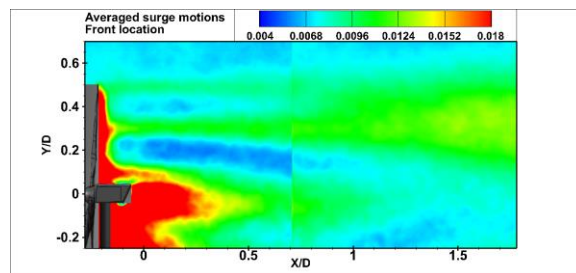
(d) Surge Motion – Front location – Averaged Motion – T.K.E.

Figure 19: Normalized Turbulent Kinetic Energy $(\frac{T.K.E.}{U_{hub}^2})$ plots in the wake of a bottom fixed turbine (a), and the front location for a turbine moving in surge motion: as it is moving with the flow (b), as it is moving into the flow (c), and the averaged forward and backward motions (d).

(a) **Bottom Fixed Turbine – U/Uhub – Center location**

(b) **Surge Motion – U/Uhub – Back location – Moving with the flow (→)**

(c) **Surge Motion – U/Uhub – Back location – Moving into the flow (←)**

(d) **Surge Motion – U/Uhub – Back location – Averaged Motion**

Figure 20: Normalized stream-wise velocity (U/Uhub) profiles in the wake of a bottom fixed turbine (a), and the back location for a turbine oscillating in surge motion: as it is moving with the flow (b), as it is moving into the flow (c), and the average of the forward and backward motion(d).

(a) Bottom Fixed Turbine – Reynolds Shear Stress and Momentum Flux – Center location
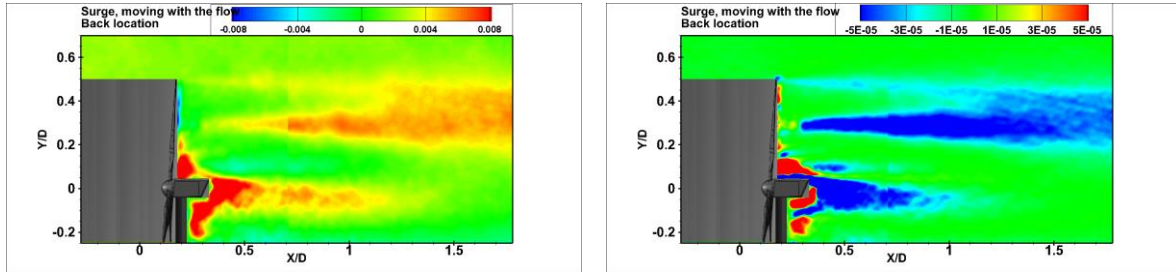
(b) Surge Motion–Reynolds Shear Stress and Momentum Flux–Back location–Moving with the flow (→)

(c) Surge Motion – Reynolds Shear Stress and Momentum Flux – Back location – Moving into the flow (←)

 (d) Surge Motion – Reynolds Shear Stress and Momentum Flux – Back location – Averaged Motion

Figure 21: Normalized Reynolds Shear Stress ($\frac{Ruv}{U_{hub}^2}$) and the Momentum Flux ($\frac{\frac{\partial U}{\partial Y}*Ruv*D}{U_{hub}^3}$) plots in the wake of a bottom fixed turbine (a), and the back location for a turbine oscillating in surge motion: as it is moving with the flow (b), as it is moving into the flow (c), and the average of the forward and backward motions (d).
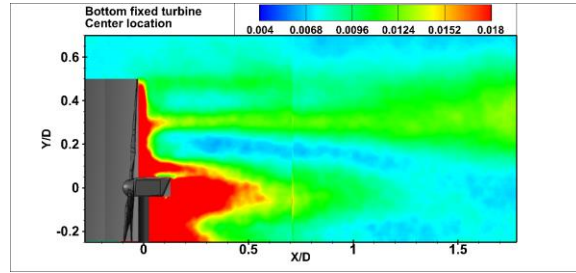
(a) Bottom Fixed Turbine – Center location – T.K.E.
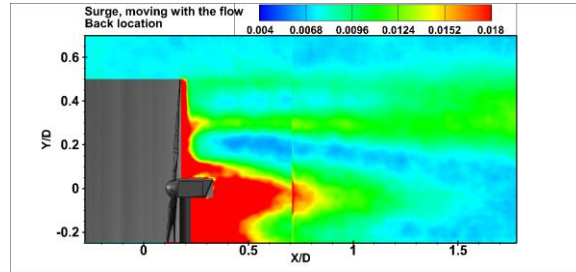
(b) Surge Motion – Back location – Moving with the flow (→) – T.K.E.
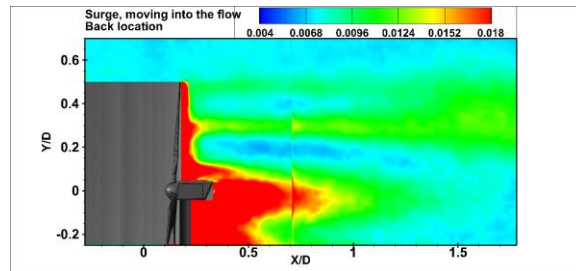
(c) Surge Motion – Back location – Moving into the flow (←) – T.K.E.
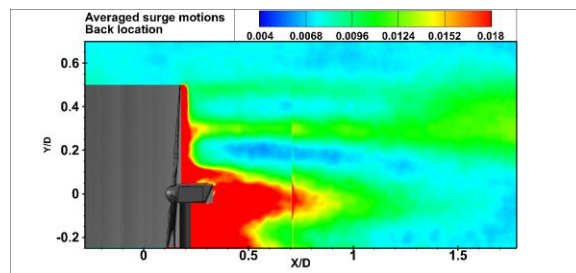
(d) Surge Motion – Back location – Averaged Motion – T.K.E.

Figure 22: Normalized Turbulent Kinetic Energy $(\frac{T.K.E.}{U_{hub}^2})$ plots in the wake of a bottom fixed turbine (a), and the back location for a turbine moving in surge motion: as it is moving with the flow (b), as it is moving into the flow (c), and the averaged forward and backward motions (d).

2.4 Results and Analysis of the Pitch Motion

The flow field (x/D < 1.8) measurements behind a wind turbine subjected to an uncoupled pitching motion were carried out by using a high-resolution PIV system, and the wake results obtained at particular pitch angles were then compared to those of a classical bottom-fixed turbine.

Out of the six degrees of freedom associated with any floating offshore wind turbines, the pitch motion is believed to be the most dominant motion. The pitch motion is defined as the angular motion of the turbine along the wind direction (the stream-wise).

The exact motions for the prototype turbine in pitch motion for the current study were determined using the previous numerical simulations results done on floating wind turbines. For the current study, the freestream velocity at the hub height of the scaled model turbine was set to 3.5 m/s. The pitching speed at the base of the tower was set to the maximum amount that the motion simulator could perform to $20 \frac{\text{deg}}{\text{s}}$ which resulted in a frequency of 0.3 Hz.

As shown in Figure 23, the PIV measurements of the wake study of a pitching turbine were performed at three critical locations; front ([-]5° ahead of the neutral location), center (0° or the neutral location), and the back location ([+]5° behind the neutral location). The flow measurements were used to quantify the differences in the wake of the pitching turbine when the aerodynamic hysteresis occurs. In the hysteresis loop, the differences in the wake flow at the same pitching condition were examined along the increasing pitch angle (i.e., the turbine is pitching *with the flow*) and the decreasing pitch angle (i.e., the turbine is pitching *into the flow*) branches.

The measurement plane was composed of two fields with an overlap of 15mm length, and two CCD cameras were used to acquire images from these fields. Two fields were then merged

in Tecplot to acquire the image in the measurement plane. Finally, ensemble averaged flow quantities, such as mean flow velocity, Reynolds stresses and Turbulence Kinetic energy, were analyzed.
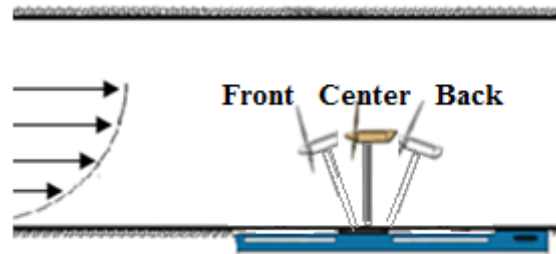
Figure 23: Illustration of turbine's oscillation in pitch motion

Figure 24, shows the four pairs of contour plots accompanied by their extracted data (at x/D = 0.8 and x/D=1.7) of the PIV measurements of the averaged stream-wise velocity component U, normalized by the hub height inflow velocity, for a classical bottom fixed turbine (a), the pitching turbine at the center location (0°) when moving with the flow (b), moving into the flow (c), and the ensemble averages of the forward and backward motions at the center location (d). Figure 29 and Figure 33 also provide the same plots corresponding to the front and back locations, respectively.

As can be seen in Figure 24, there is clear evidence of the deficit in the velocity in the wake of both; the bottom fixed turbine and the pitching turbine. This deficit is the result of energy extraction by the turbine itself. Double peaks are observed and understood as characteristic of the near wake profiles (X/D <1). But as we go farther down in the wake (X/D >1), the double peaks die out and become just a single peak. This single peak eventually dies out in approximately 15~20 diameter downstream of the turbine, where the flow gains its fullest momentum and becomes the undisturbed flow again. There is some overshoot at the top region of the profiles in the near wake regions, corresponding to the plots of both turbines

which suggests that the flow is accelerating at near top-tip of the blade, and also could be an evidence of the blockage effect caused by the existence of the turbine itself.

From the extracted data of Figure 24b and 24c, during the pitching motion, as the turbine is at the center location and is moving with the flow (to the right), it's wake tends to accelerate when compared to the wake of the bottom fixed turbine, suggesting a reduced energy extraction by the rotor. This trend is anticipated to become more pronounced as we go down farther in the wake. However, as the turbine is moving into the flow (to the left), the wake of the pitching turbine becomes very similar to the wake of the bottom-fixed turbine. Therefore, with the current prescribed range of motions, the current pitching velocity, and the frequency, there would be no significant difference between the power extraction by the pitching turbine at the center location and the bottom-fixed turbine (see Figure 24d).

However, more significant differences between the bottom-fixed turbine and the pitching turbine at pitching angles of -5° and 5° were observed in the vicinity of the rotor, just behind the nacelle. The downward pitching (i.e. pitch angle of -5°) of the wind turbine was found to cause stronger velocity deficits in the vertical range of $y/D = -0.1$ and $y/D = 0.2$ at a downstream location of $x/D = 0.8$ in comparison to the fixed turbine case; whereas the upward pitching motion (i.e. pitch angle of 5°) was found to have the exact opposite effect on the velocity profiles. Furthermore, the decrease in the velocity deficit for the upward pitching motion is slightly higher than the increase in the velocity deficit for the downward pitching motion. Moreover, the decrease in the velocity deficit was found to expand further in the vertical direction above the hub height with the hub height ($y/D = 0$) being the location where maximum flow velocity enhancement occurs at $x/D = 0.8$.

The typical wake pattern of a classical (fixed) horizontal axis wind turbine was found to be very similar to the pitching turbine, between the pitch angles of -5° and 5°, contrary to the findings of Rockel et al. (2014). Rockel determined that the pitching motion would significantly change the wake flow pattern behind the oscillating turbine, causing an upward skewed (approximately 3°) flow. However, their results were based on a pitching angle of approximately 18°, which would not be reasonable under the normal operating condition of a floating turbine.

Figure 25, presents the contours of the normalized lateral component of the velocity (V/Uhub) for both the bottom fixed turbine and the pitching turbine at the center location, as it is moving with the flow and into the flow. From the contour plots it is clearly evident that the motion of the turbine greatly influences the vertical movements of the flow in the wake of the turbine. Contrary to the surge motion, for the pitching motion, as the turbine is moving with the flow, it generates a higher rate of vertical motion in the wake compared to the bottom fixed turbine. However, as the turbine is moving into the flow, it generates lesser amount of motion in vertical direction, when compared to the bottom-fixed turbine.

When the turbine is pitched to the front location (as shown in Figure 30), and as the turbine is moving with the flow, it generates a higher rate of vertical motion in the wake, compared to the bottom-fixed turbine. As the turbine is moving into the flow, it also generates higher amount of motion in vertical direction, when compared to the bottom-fixed turbine. However, when the turbine is at the back location (as shown in Figure 34), the vertical motion of the flow in the wake would behave exactly opposite to the case when the turbine was in the front location.

Figure 26, shows the Reynolds shear stress ($\tau = \frac{-u'v'}{U_{hub}^2}$) and the momentum flux ($\frac{\frac{\partial U}{\partial Y} * Ruv * D}{U_{hub}^3}$) plots. The Reynolds shear stress deals with the transport of momentum from high energy flow above the rotor to the lower energy area of the wake region. The momentum flux which is the rate of change of momentum is also another indicator on how fast the higher energy flow above the turbine is being fed into the lower energy area of the wake region. Therefore, both the Reynolds shear stress and momentum flux are directly related on how fast the wake is recovering.

The momentum flux observed in the top tip (shear) layer of the oscillating turbine, and the areas covered by negative fluxes and the magnitudes of these fluxes were found to increase slowly as the wake flow advects downstream for the floating turbine. The negative valued momentum fluxes could be used as an indicator of the flow into the wake centerline, which is the result of strong mixing. Therefore, the high momentum flow above the shear layer could mix with the wake flow characterized with greater velocity deficits. These momentum fluxes could play a significant role in wind farms having clusters of wind turbines by accelerating the wake recovery in the far wake region. As a result, downstream turbines could extract more energy from the disturbed flow.

Figure 27, shows the turbulent kinetic energy ($T.K.E. = \frac{1}{2}\frac{[u'^2 + v'^2]}{U_{hub}^2}$). T.K.E. is the kinetic energy per unit mass associated with the eddies in the turbulent flows. T.K.E. deals with the diffusivity effect which is responsible for enhanced mixing. By studying T.K.E., one can determine on how fast the wake is recovering. The fluctuating components of the oncoming boundary layer flow influences the turbulent wake flow structure significantly. For a uniform flow, mean shear distribution in the turbine wake could be axisymmetric with strong shear layer (associated with TKE production) at the levels of bottom-tip and top-tip. However, for

an oncoming boundary layer flow with non-uniform mean flow velocity distribution, previous experimental and numerical studies showed that maximum TKE production would occur at the top-tip level as a result of strong shear-produced turbulence and turbulent fluxes (Hu et al., 2012; Zhang et al., 2012; Porte-Agel et al., 2011; Wu et al., 2012). Turbulent fluxes produced due to wake induced turbulence were found to play an important role on the entrainment of energy from the flow above the wind farm (Meyers and Meneveau, 2013).

As can be seen in Figure 26 and Figure 27, there are relatively higher amount of Reynolds shear stress, momentum flux, and T.K.E. associated with the pitching turbine at the center location, as it is moving into the flow when compared to the bottom fixed turbine, and lower amount associated with the pitching turbine moving with the flow. However, the differences are just too little to have any significant contribution in the wake recovery of the pitching turbine. Therefore, the wake of the pitching turbine at the center location would travel about the same distance as the wake of a traditional bottom fixed turbine.

As can be seen in Figure 31 and Figure 32, there are substantially higher amount of Reynolds shear stress, momentum flux, and T.K.E. associated with the pitching turbine at the front location, regardless of which direction the turbine is oscillating when compared to the bottom fixed turbine. Therefore, the wake of the pitching turbine at the front location would travel much shorter before dissipating, when compared to the wake of a traditional bottom fixed turbine.

As the oscillating turbine pitches upwards (from -5° to 5°), the top tip shear layer was found to expand more slowly. At a pitching angle of -5° (front location), the shear layer expansion was observed to start at approximately x/D = 0.5; whereas it was observed to start after x/D = 1.2 at a pitching angle of 5° (back location). In case of centered position (pitch angle of 0°) of the floating turbine, shear layer expansion was found to start after x/D = 1.0 analogous to the

fixed turbine case. As can be seen in Figure 35 and Figure 36, there are substantially lower amount of Reynolds shear stress, momentum flux, and T.K.E. associated with the pitching turbine at the back location, regardless of which direction the turbine is oscillating when compared to the bottom fixed turbine. Therefore, the wake of the pitching turbine at the back location would travel much longer before dissipating, when compared to the wake of a traditional bottom fixed turbine.

Rockel et al. (2014) also found that the classical bottom fixed turbine with its rigid structure would enhance mixing thereby providing a faster recovery in the shear layer of the wake when compared to the pitching turbine. Therefore, the far wake region behind the fixed turbine and the pitching turbine would significantly differ, affecting the performance of the downwind turbines operating in the wake of the front row turbines. The power extracted by the downwind pitching turbines would be 14% - 16% lower (with front row turbines pitching to approximately 18°) than the turbines behind the bottom-fixed turbine.

However, recent study showed that the reduced range of the pitching angle for the floating turbine would provide almost the same far wake velocity pattern as for the bottom-fixed turbine. Therefore, downwind turbines behind the fixed and pitching turbine would perform almost the same.

Figure 28, show the normalized phase-locked $(\frac{w_z D}{U_{hub}})$ vorticity distributions in the wake of the bottom fixed turbine and the turbine oscillating in surge motion at a phase angle of $\theta = 0°$. The vorticity (w_z) values were derived from the phase locked velocity distributions in the streamwise and vertical directions by using the expression $w_z = \frac{dV}{dx} - \frac{dU}{dy}$. The phase-locked PIV measurements could be used to identify the unsteady vortex structures (i.e., tip and root vortices, and vortices formed within the nacelle boundary layer) generated in the wake.

As shown in Figure 28, the tip vortices were formed in the strong shear layer located at the uppermost level of the wake. Interestingly, an additional array of concentrated vortices were found to shed from the inboard section located at approximately 50% - 60% of the blade span. Furthermore, these vortex structures were found to expand outwards as they convect downstream and finally merge with those shedding from the blade tips. Moreover, these additional array of concentrated vortices were found to be larger and stronger than those generated by the blade tips. The vortices formed within the nacelle boundary layer with those shedding from the blade root section were found to dissipate much faster than those generated at the tip and inboard section of the blade.

There is a strong connection between the tip vortex breakdown and the shear layer expansion. Lignarolo et al. (2013) showed that tip-vortices could act against the turbulent mixing; however, the break-down of these vortices could enhance turbulent mixing.

The effect of the hysteresis loop on the evolution (i.e., formation, shedding and dissipation) of the unsteady vortex structures for the bottom fixed turbine and the oscillating turbine are shown in Figure 28. The hysteresis loop was found to make no significant changes on the evolution of the unsteady vortex structures. However, slight changes in the shape and magnitude of the vortex structures can be seen. Furthermore, contrary to the bottom fixed turbine, the vortices shedding from the inboard and tip sections of the turbine blade were found to break-down/dissipate faster for the oscillating turbine. However, the behavior of the vortices shedding from the nacelle boundary layer and blade root section was pretty similar for the fixed and the turbine in pitching motion.

(a) Bottom Fixed Turbine – U/Uhub – Center location

(b) Pitch Motion – U/Uhub – Center location – Moving with the flow (→)
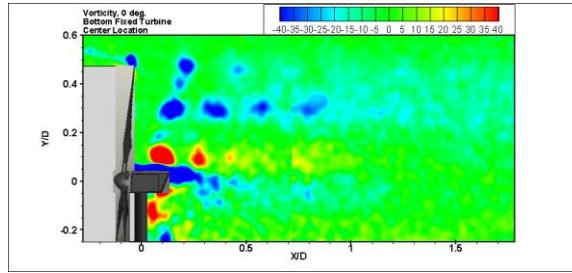

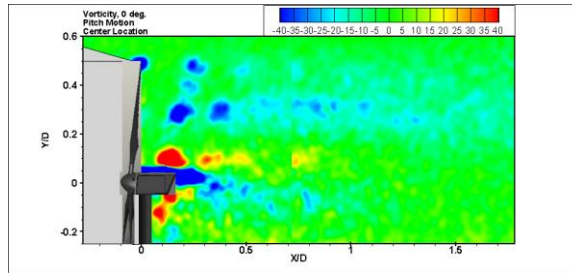(c) Pitch Motion – U/Uhub – Center location – Moving into the flow (←)

(d) Pitch Motion – U/Uhub – Center location – Averaged motion
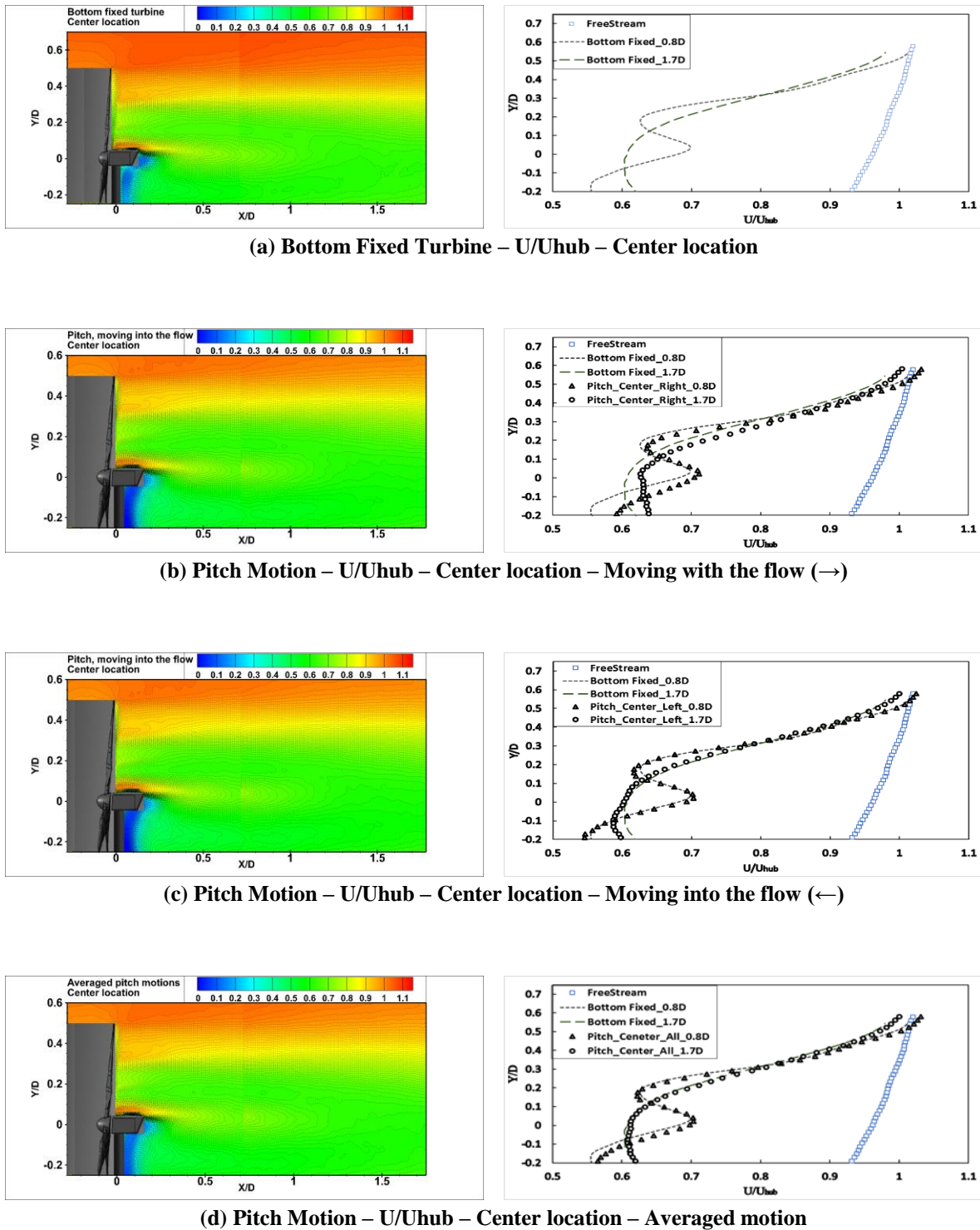
Figure 24: Normalized stream-wise velocity (U/Uhub) profiles in the wake of a bottom fixed turbine (a), the center location for a pitching turbine as it is moving with the flow (b), as it is moving into the flow (c), and the averaged of forward and backward motion (d).
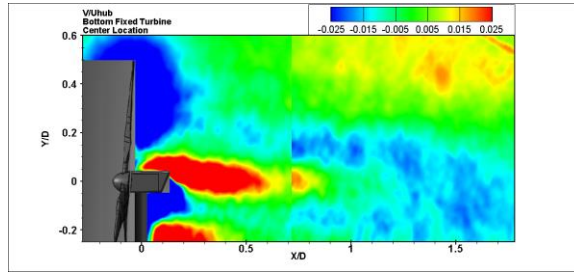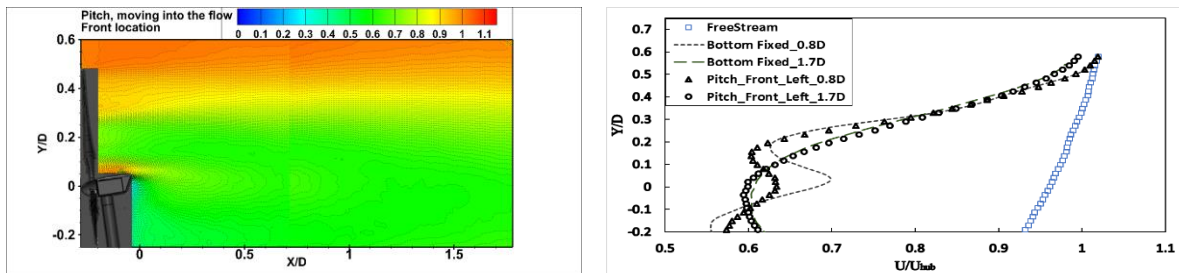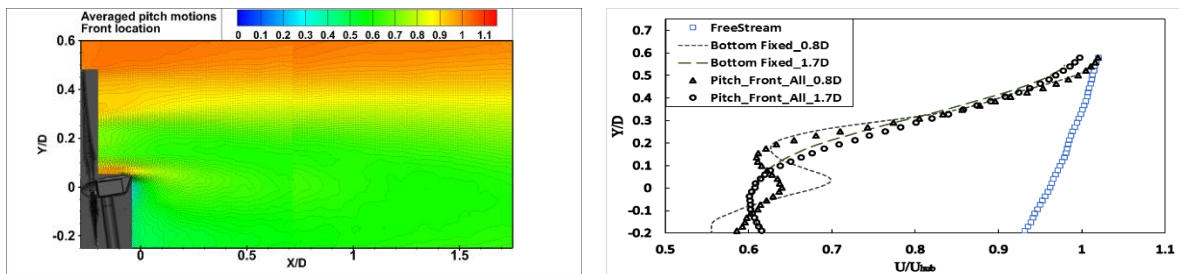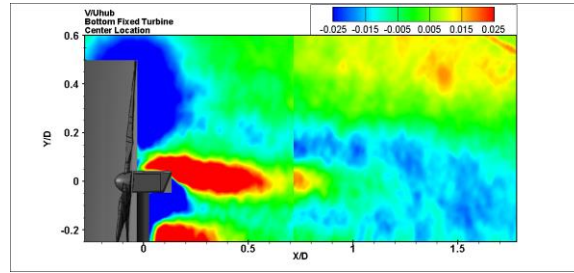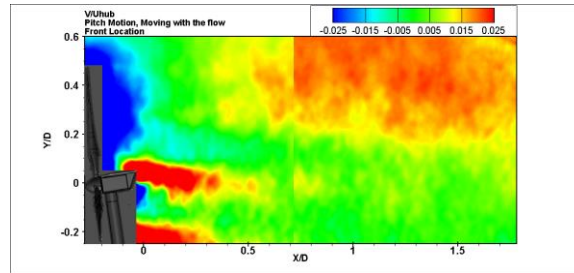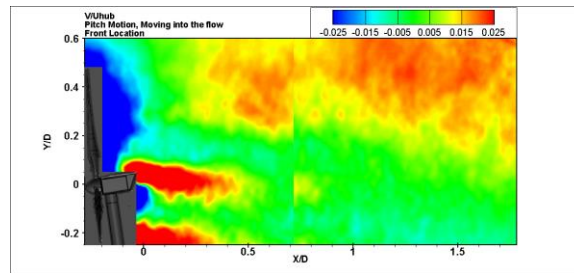
(a) Bottom Fixed Turbine – V/Uhub – Center location
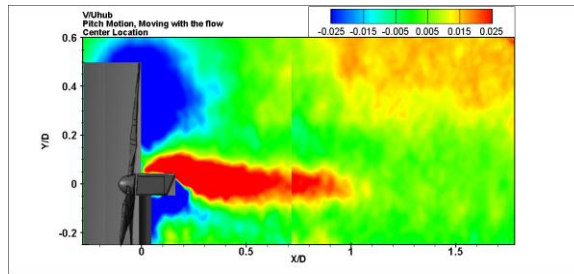
(b) Pitch Motion – V/Uhub – Center location – Moving with the flow (→)
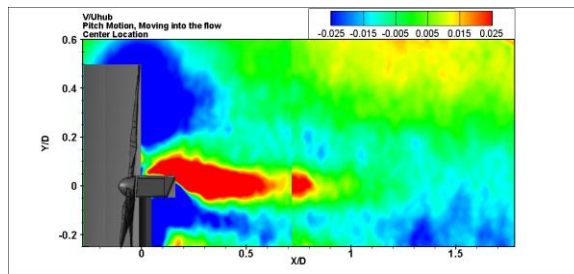
(c) Pitch Motion – V/Uhub – Center location – Moving into the flow (←)
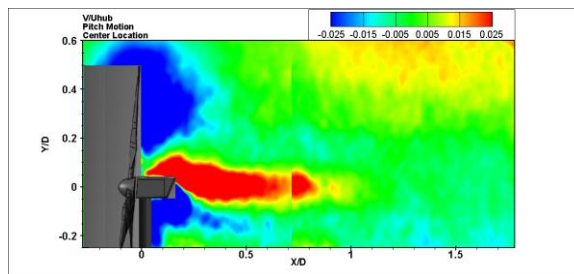
(d) Pitch Motion – V/Uhub – Center location – Averaged motion

Figure 25: Normalized lateral velocity (V/Uhub) profiles in the wake of a bottom fixed turbine (a), and the center location for a turbine oscillating in pitch motion: as it is moving with the flow (b), as it is moving into the flow (c), and the average of the forward and backward motions (d).
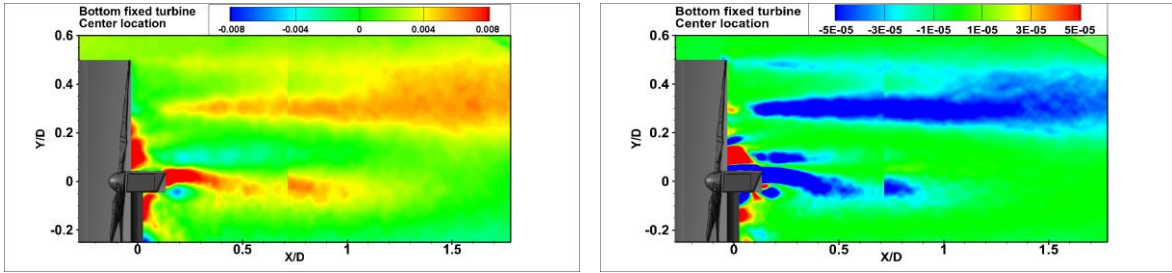
(a) Bottom Fixed Turbine – Reynolds Shear Stress and Momentum Flux – Center location
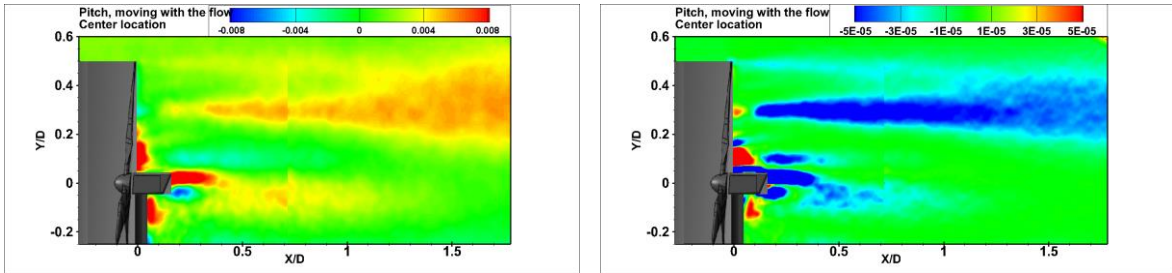
(b) Pitch Motion–Reynolds Shear Stress and Momentum Flux–Center location–Moving with the flow (→)

(c) Pitch Motion–Reynolds Shear Stress and Momentum Flux–Center location–Moving into the flow (←)

(d) Pitch Motion–Reynolds Shear Stress and Momentum Flux–Center location–Averaged Motion

Figure 26: Normalized Reynolds Shear Stress ($\frac{Ruv}{U_{hub}^2}$) and the Momentum Flux ($\frac{\frac{\partial U}{\partial Y}*Ruv*D}{U_{hub}^3}$) plots in the wake of a bottom fixed turbine (a), and the center location of a pitching turbine as it is moving with the flow (b), as it is moving into the flow (c), and the averaged of forward and backward motion (d).
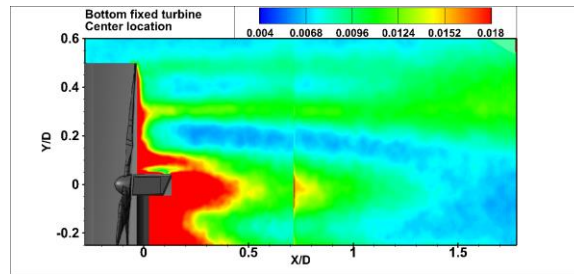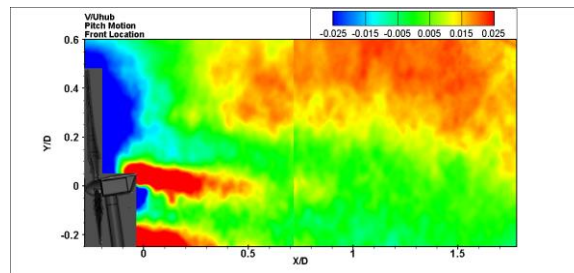
(a) Bottom Fixed Turbine – Center location – T.K.E.
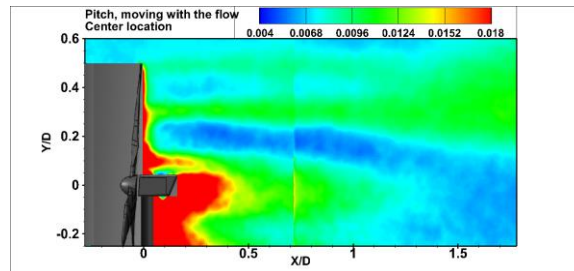
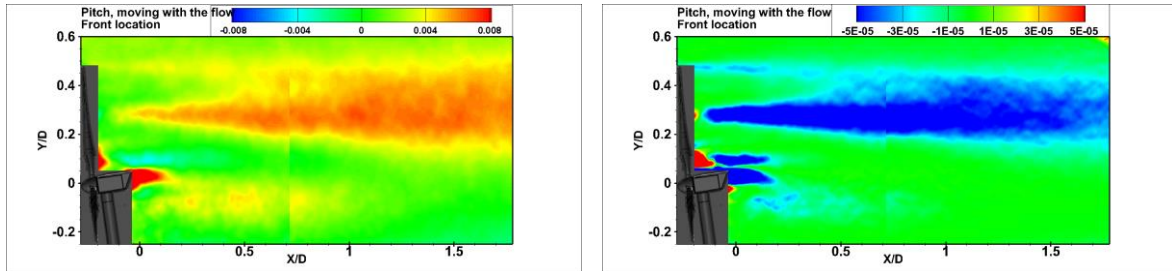**(b) Pitch Motion – Center location – Moving with the flow (→) – T.K.E.**
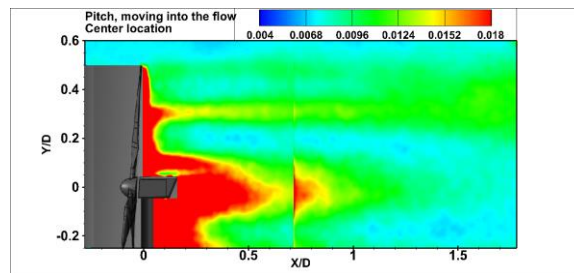
(c) Pitch Motion – Center location – Moving into the flow (←) – T.K.E.
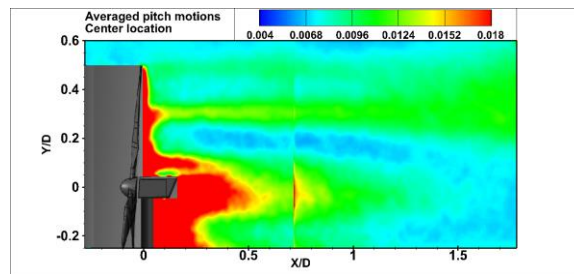
(d) Pitch Motion – Center location – Averaged Motion – T.K.E.

Figure 27: Normalized Turbulent Kinetic Energy $(\frac{T.K.E.}{U_{hub}^2})$ plots in the wake of a bottom fixed turbine (a), and the center location of a pitching turbine as it is moving with the flow (b), as it is moving into the flow (c), and the average of forward and backward motion (d).
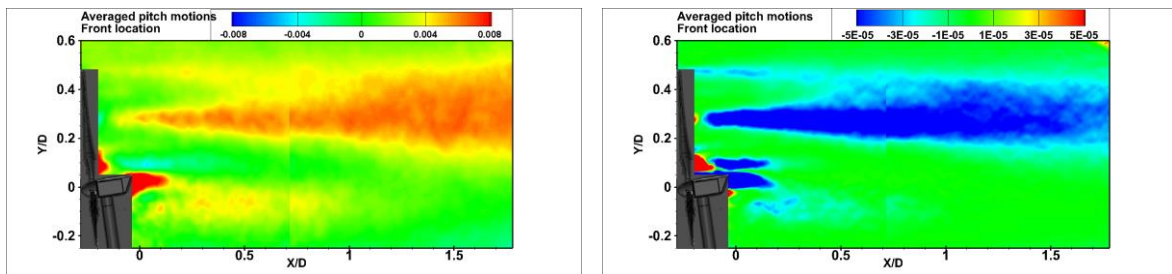
(a) Bottom fixed turbine – Vorticity – Center location

(b) Pitch motion – Averaged Motion – Vorticity – Center location
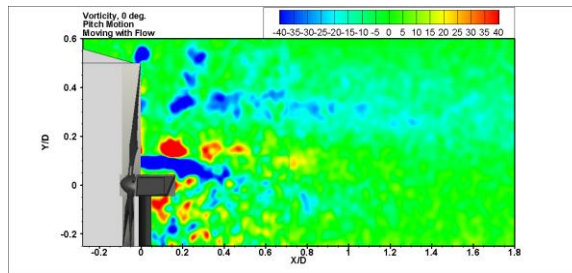
(c) Pitch Motion – Moving into the flow – Vorticity – Center location (→)
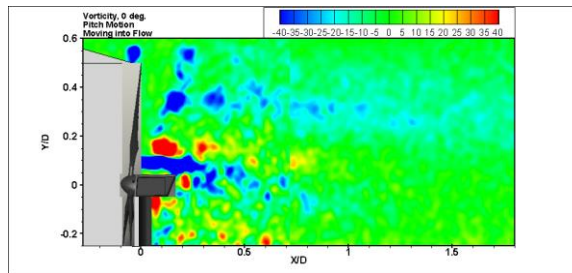
(d) Pitch motion – Moving with the flow – Vorticity – Center location (←)

Figure 28: Normalized vorticity distribution $(\frac{w_z \, D}{U_{hub}})$ plots in the wake of a bottom fixed turbine (a), and the center location for the pitching turbine: the averaged vorticity of forward and backward motions (b), as it is moving with the flow (c), and as it is moving into the flow (d).
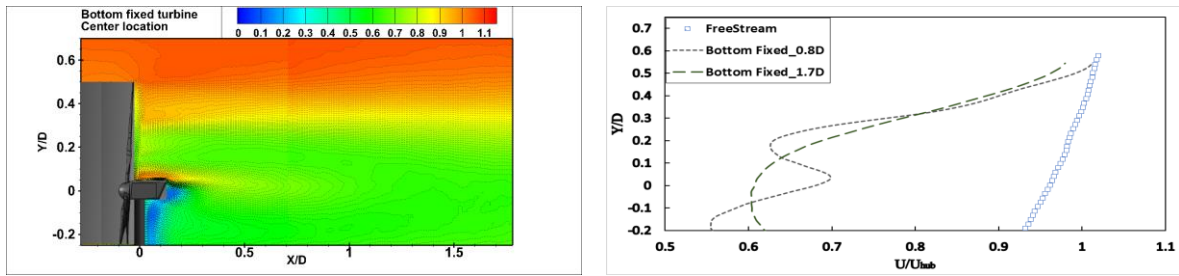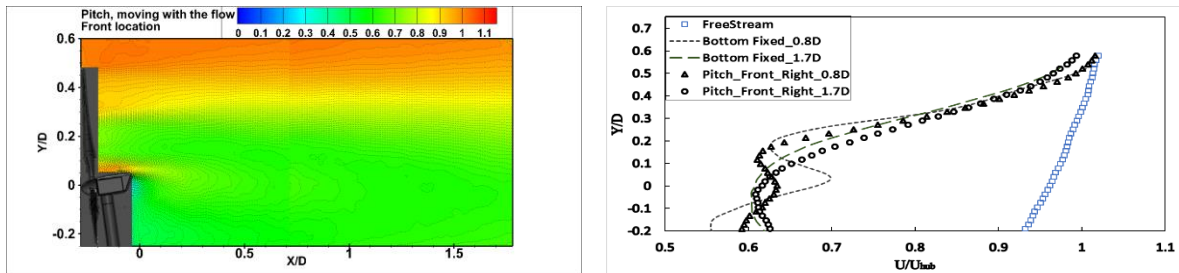
(a) Bottom Fixed Turbine – U/Uhub – Center location

(b) Pitch Motion – U/Uhub – Front location – Moving with the flow (→)

(c) Pitch Motion – U/Uhub – Front location – Moving into the flow (←)

(d) Pitch Motion – U/Uhub – Front location – Averaged motion

Figure 29: Normalized stream-wise velocity (U/Uhub) profiles in the wake of a bottom fixed turbine (a), the front location for a pitching turbine as it is moving with the flow (b), as it is moving into the flow (c), and the averaged of forward and backward motion (d).
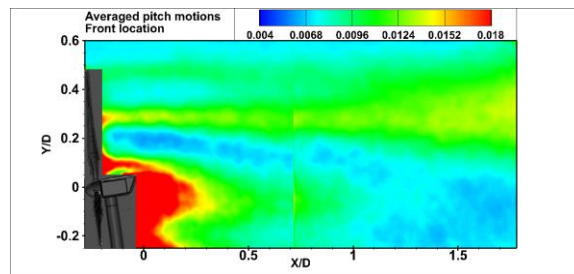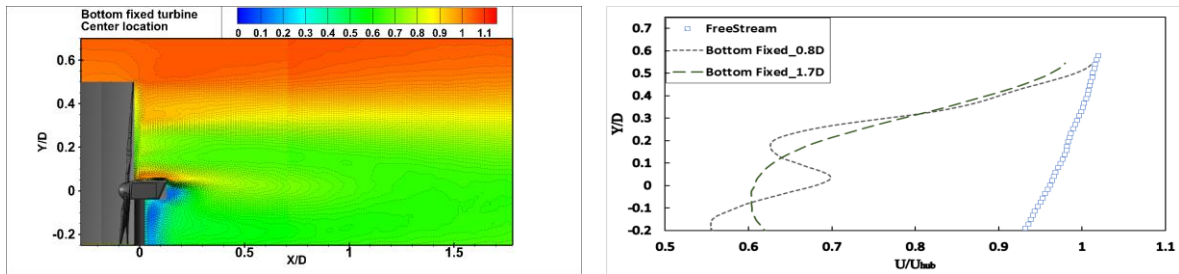
(a) Bottom Fixed Turbine – V/Uhub – Center location

(b) Pitch Motion – V/Uhub – Front location – Moving with the flow ($\rightarrow$)

(c) Pitch Motion – V/Uhub – Front location – Moving into the flow ($\leftarrow$)

(d) Pitch Motion – V/Uhub – Front location – Average motion

Figure 30: Normalized lateral velocity (V/Uhub) profiles in the wake of a bottom fixed turbine (a), and the front location for a turbine oscillating in pitch motion: as it is moving with the flow (b), as it is moving into the flow (c), and the average of the forward and backward motions (d).
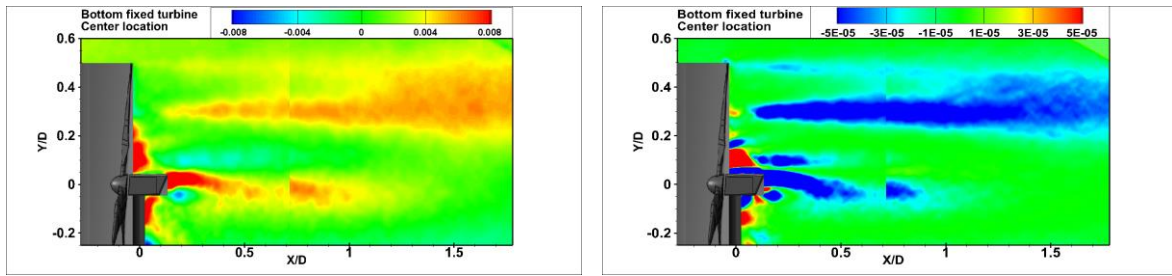
(a) Bottom Fixed Turbine – Reynolds Shear Stress and Momentum Flux – Center location

(b) Pitch Motion – Reynolds Shear Stress and Momentum Flux–Front location–Moving with the flow (→)

(c) Pitch Motion – Reynolds Shear Stress and Momentum Flux–Front location–Moving into the flow (←)

(d) Pitch Motion – Reynolds Shear Stress and Momentum Flux –Front location–Averaged Pitch Motion

Figure 31: Normalized Reynolds Shear Stress ($\frac{Ruv}{U_{hub}^2}$) and the Momentum Flux ($\frac{\frac{\partial U}{\partial Y}*Ruv*D}{U_{hub}^3}$) plots in the wake of a bottom fixed turbine (a), and the front location of a pitching turbine as it is moving in with the flow (b), as it is moving into the flow (c), and the averaged of forward and backward motion (d).
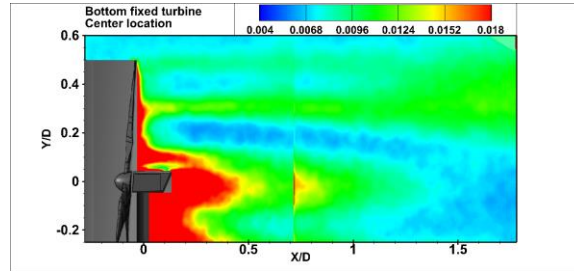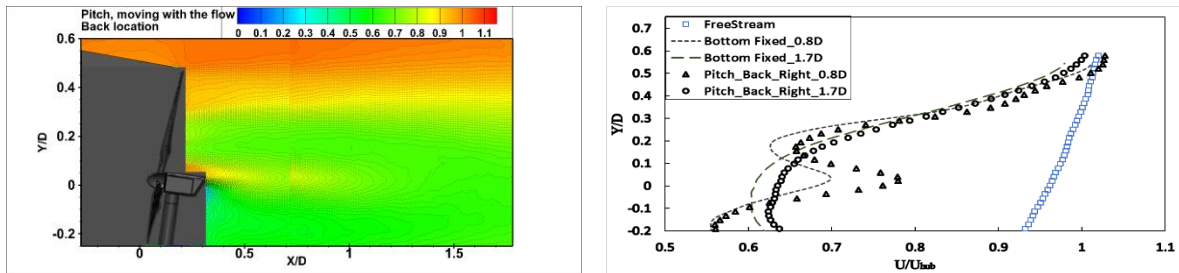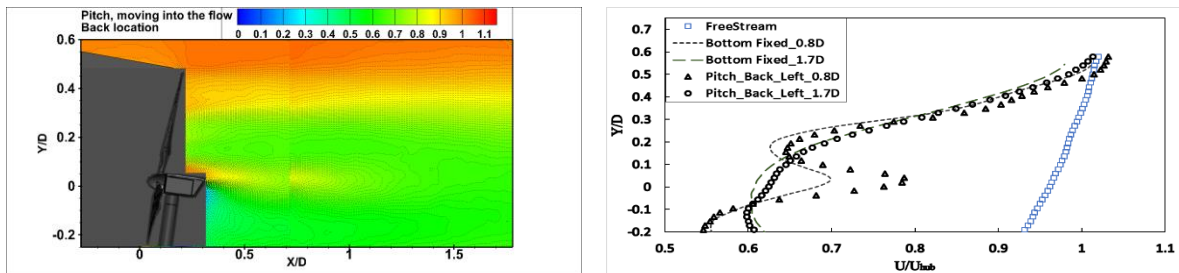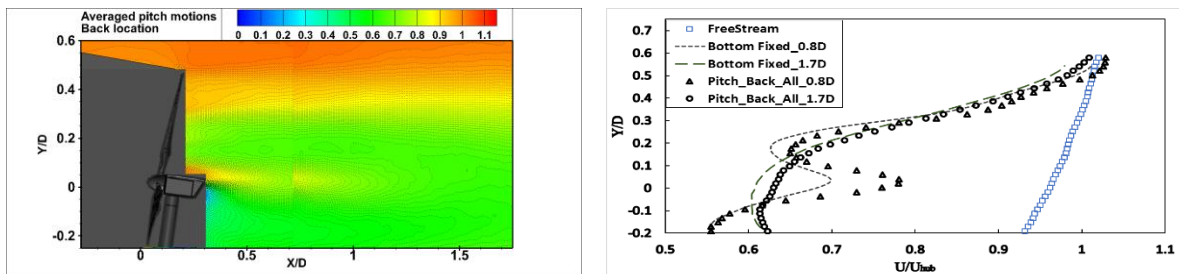
(a) Bottom Fixed Turbine – Center location – T.K.E.
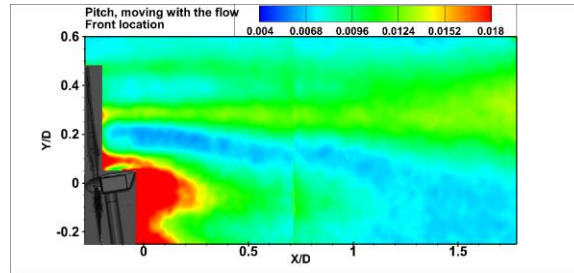
(b) Pitch Motion – Front location – Moving with the flow (→) – T.K.E.
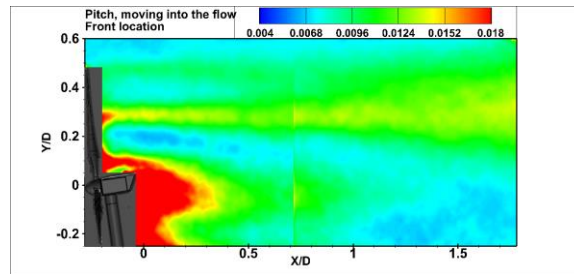
(c) Pitch Motion – Front location – Moving into the flow (←) – T.K.E.

(d) Pitch Motion – Front location – Averaged Pitch Motion – T.K.E.

Figure 32: Normalized Turbulent Kinetic Energy $\left(\frac{T.K.E.}{U_{hub}^2}\right)$ plots in the wake of a bottom fixed turbine (a), and the front location of a pitching turbine as it is moving with the flow (b), as it is moving into the flow (c), and the average of forward and backward motion (d).

(a) Bottom Fixed Turbine – U/Uhub – Center location

(b) Pitch Motion – U/Uhub – Back location – Moving with the flow (→)

(c) Pitch Motion – U/Uhub – Back location – Moving into the flow (←)

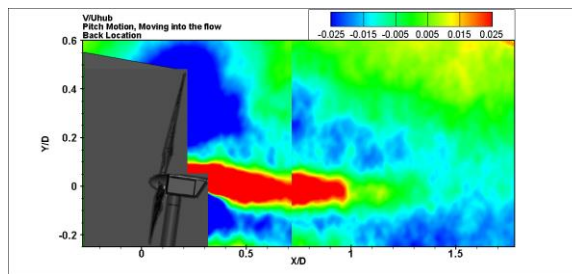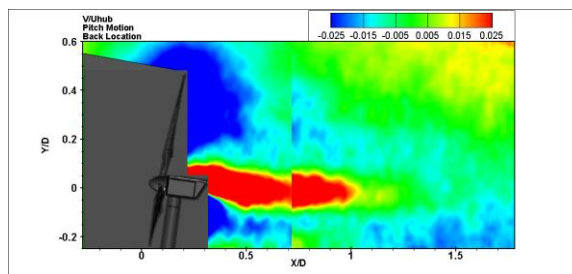
(d) Pitch Motion – U/Uhub – Back location – Averaged motion

Figure 33: Normalized stream-wise velocity (U/Uhub) profiles in the wake of a bottom fixed turbine (a), the back location for a pitching turbine as it is moving with the flow (b), as it is moving into the flow (c), and the averaged of forward and backward motion (d).
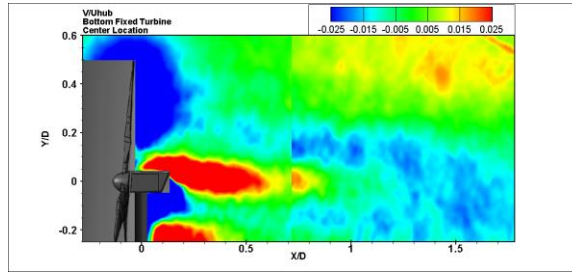
(a) Bottom Fixed Turbine – V/Uhub – Center location
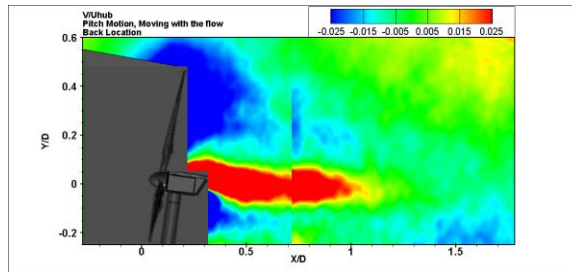
(b) Pitch Motion – V/Uhub – Back location – Moving with the flow (→)

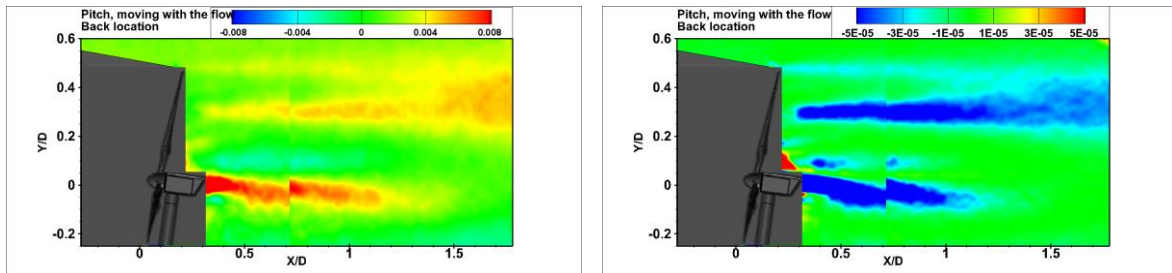**(c) Pitch Motion – V/Uhub – Back location – Moving into the flow (←)**

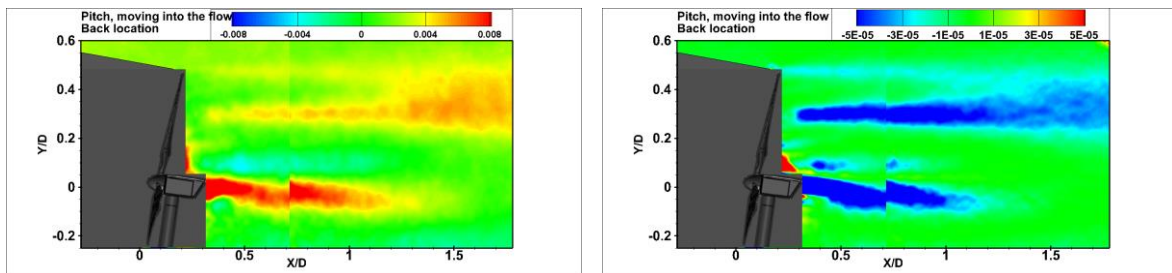**(d) Pitch Motion – V/Uhub – Back location – Average motion**

Figure 34: Normalized lateral velocity (V/Uhub) profiles in the wake of a bottom fixed turbine (a), and the back location for a turbine oscillating in pitch motion: as it is moving with the flow (b), as it is moving into the flow (c), and the average of the forward and backward motions (d).
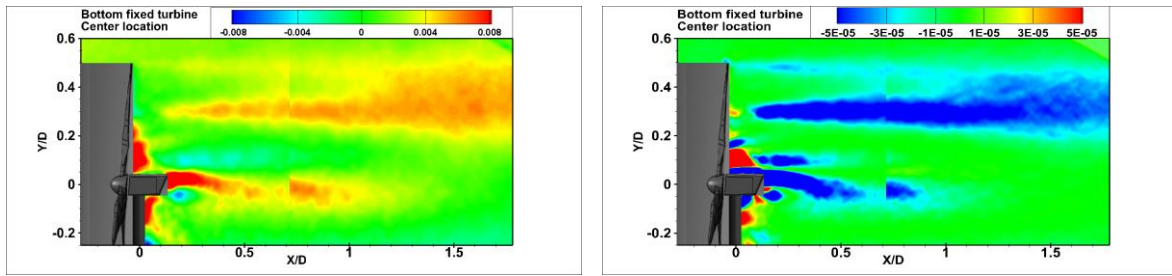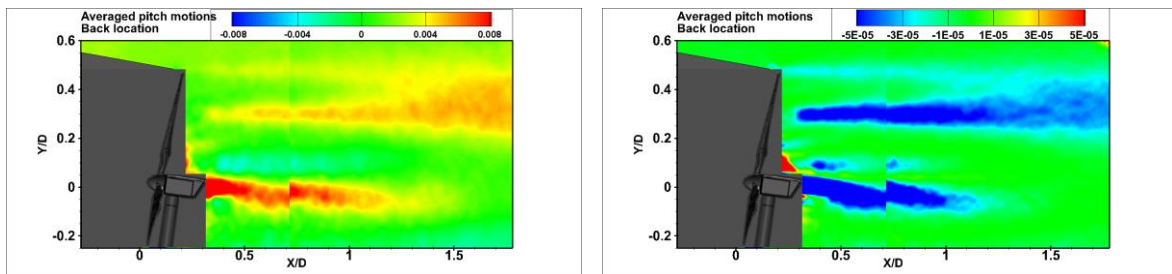
(a) Bottom Fixed Turbine – Reynolds Shear Stress and Momentum Flux – Center location

**(b) Pitch Motion–Reynolds Shear Stress and Momentum Flux–Back location–Moving with the flow (→)**

(c) Pitch Motion–Reynolds Shear Stress and Momentum Flux–Back location–Moving into the flow (←)


(d) Pitch Motion–Reynolds Shear Stress and Momentum Flux–Back location–Moving Pitch Motion

**Figure 35: Normalized Reynolds Shear Stress ($\frac{Ruv}{U_{hub}^2}$) and the Momentum Flux ($\frac{\frac{\partial U}{\partial Y}*Ruv*D}{U_{hub}^3}$) plots in the wake of a bottom fixed turbine (a), and the back location of a pitching turbine as it is moving with the flow (b), as it is moving into the flow (c), and the averaged of forward and backward motion (d).**

65
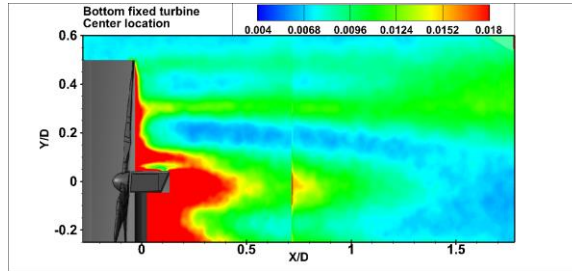
(a) Bottom Fixed Turbine – Center location – T.K.E.
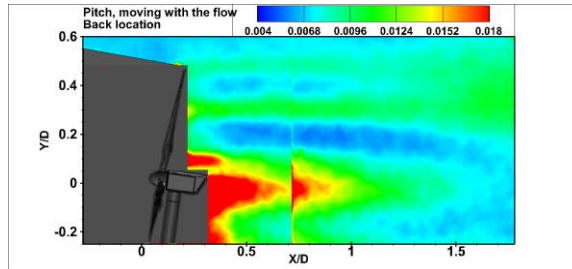
(b) Pitch Motion – Back location – Moving with the flow (→) – T.K.E.
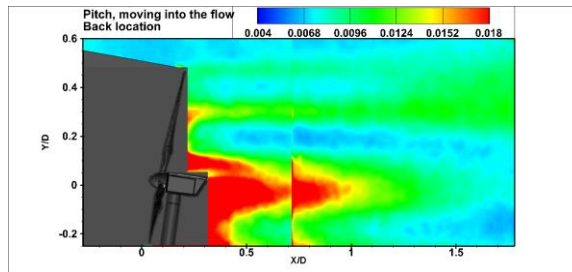
(c) Pitch Motion – Back location – Moving into the flow (←) – T.K.E.

(d) Pitch Motion – Back location – Averaged Pitch Motion – T.K.E.

Figure 36: Normalized Turbulent Kinetic Energy $(\frac{T.K.E.}{U_{hub}^2})$ plots in the wake of a bottom fixed turbine (a), and the back location of a pitching turbine as it is moving with the flow (b), as it is moving into the flow (c), and the average of forward and backward motion (d).
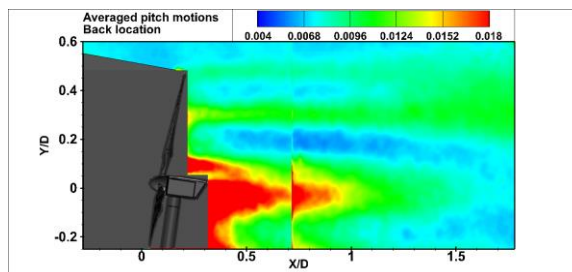
2.5 Results and Analysis of the Heave Motion

The flow field (x/D < 1.8) measurements behind a wind turbine subjected to only heave motion was carried out by using a high-resolution PIV system. The heave motion is defined as the linear translation of the turbine in vertical direction, perpendicular to the incoming flow. As shown in Figure 37, the turbine was set to oscillate in heave motion with a displacement range of $\binom{+}{-}$ 2 cm about the neutral location. The three critical locations for the current study of the heave motion include; upper location (2 cm above of the neutral location), center (the neutral location), and the lower location (2 cm below the neutral location).

The range of the vertical motion (~ 4 cm) for the heaving turbine corresponds to 1/6.75 of the turbine hub height. The turbine was set to heave within this range at approximately 0.32 Hz. (i.e., at a speed of 10 cm/s). The flow measurements were also used to quantify the differences in the wake of the heaving turbine when the aerodynamic (wake) hysteresis occurs. In the hysteresis loop, the differences in the wake flow at the same vertical position of the heaving turbine were examined along the increasing vertical path (i.e., the turbine is moving upwards from -2 cm to +2 cm) and decreasing vertical path (i.e., the turbine is moving downwards from +2 cm to -2 cm) branches.
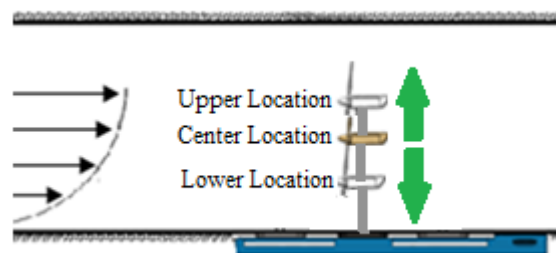

Figure 37: Illustration of turbine's oscillation in heave motion

The measurement plane was composed of two fields with an overlap of 15mm length, and two CCD cameras were used to acquire images from these fields. The two fields were then

merged in Tecplot to acquire the image in the measurement plane. Finally, ensemble averaged flow quantities, such as mean flow velocity, Reynolds stresses and Turbulence Kinetic energy, were analyzed.

Figure 38, shows the contour plots of the averaged stream-wise velocity (U/Uhub) profiles in the wake of a bottom fixed turbine (a), and the center location for a turbine oscillating in heave motion: as it is moving upward (b), as it is moving downward (c), and the averaged of the upward and downward motions (d). Each of the contour plots are accompanied by their extracted data (at x/D = 0.8 and x/D=1.5) of the PIV measured normalized stream-wise velocities.

As can be seen in Figure 38, there is clear evidence of the deficit in the velocity in the wake of both; the bottom fixed turbine and the oscillating turbine. This deficit is the result of the energy extraction by the turbine itself. Double peaks are observed and understood as characteristic of the near wake profiles (X/D <1). But as we go farther down in the wake (X/D >1), the double peaks die out and become just a single peak. This single peak eventually dies out in approximately 15~20 diameter downstream of the turbine, where the flow gains its fullest momentum and becomes the undisturbed flow again. There is some overshoot at the top region of the profiles in the near wake regions which suggests that the flow is accelerating at near top-tip of the blade, and also could be an evidence of the blockage effect caused by the existence of the turbine itself.

Figure 38, also provide valuable insights about the wake patterns behind a turbine as it undergoes a pure heaving motion. The study of such behavior can be approached in two different ways: statically and dynamically. The static approach would only consider the frozen images of the oscillating turbine at specific heights, and investigates the wake profiles and compare them with the wake of a classical bottom fixed turbine. However, in the dynamic

approach, one would take into account the continuous and periodic motion associated with the heaving motion within an acceptable vertical range. In reality, this kind of motion can induce fluctuations in the power output, thereby lowering the power quality of the floating offshore wind turbines. The periodic heave motion would also influence the dynamic loading associated with the floating wind turbines. The tendency of the floating turbine to go up or down (i.e., the hysteresis loop) to specific heights during the heave motion could have a significant impact on the wake patterns as well.

From the static point of view, the heave motion can either increase or decrease the hub (reference) height of the wind turbine. The turbine was set to heave within preselected (acceptable) limits (i.e., ±2 cm). The elevated/lowered turbine could be treated as the fixed turbine with increased/reduced hub height. Therefore, the typical wake pattern behind a wind turbine in pure heaving motion was found to be very similar to the wake of a classical bottom fixed turbine. The only difference observed is that the wake stream-wise velocity profile is shifted upwards at the upper location (see Figure (41d)), and it is shifted downwards at the lower location (see Figure (44d)). The upward/downward shifts observed in the velocity profiles, can be clearly seen in both downstream locations of $x/D = 0.8$ and $x/D = 1.5$.

The elevated turbine (i.e., at the upper location) could experience higher wind speeds so that its power production is expected to be higher compared to the fixed turbine. The power production from the wind turbine is strongly linked with the velocity deficits observed in its wake. Therefore, as shown in Figure (41d), an upward shift on the velocity profile would indicate greater velocity deficits at the same height. The gap between velocity deficits was also found to be more pronounced towards the mid and tip sections (i.e., $0.2 < y/D < 0.5$) of the blade, since these sections are responsible for the power extraction from the incoming wind. However, as shown in Figure (44d), a downward shift would indicate less power extraction

from the incoming wind, thereby causing smaller velocity deficits. This can be associated with the less power available in the wind, due to the fact that the heaving turbine is dropped (i.e., to the lower location), hence operating at a region of the boundary layer where wind speeds are significantly lower.

From the dynamic point of view, the continuous up and down movement of a wind turbine during the heave motion can significantly change the wake structure. As the oscillating turbine heaves within the preselected vertical limits, the frozen images of the moving turbine were also taken at the specific heights similar to the static case. However, as opposed to the static case, the oscillating turbine was either moving along the increasing vertical path (i.e., the turbine is moving upwards from -2 cm to +2 cm) or moving along the decreasing vertical path (i.e., the turbine is moving downwards from +2 cm to -2 cm) at that specific vertical position. Therefore, the oscillating wind turbine was put in a hysteresis loop, and the effects of the hysteresis on the wake dynamics were investigated.

When the oscillating turbine is moving upward to the upper location, its wake was found to deflect downwards; whereas its wake was found to deflect upwards as the turbine was moving downwards from the upper location. This effect (hysteresis) can be clearly seen from Figure (38b, 38c), Figure (41b, 41c) and Figure (44b, 44c). When the turbine is moving upward to the upper location, the difference between the velocity profiles (the vertical gap due to the upward shift), between the heaving turbine and the bottom fixed turbine was found to become narrow. This is an indication of the deflection of the wake towards the wake centerline (see Figure (41b)). However, this gap was found to become wider as the oscillating turbine was moving downwards from the upper location indicating the wake deflection towards the outer wake (see Figure (41c)). These effects would be the opposite in the case of the lower location (i.e., at -2 cm) since the vertical gap was formed due to the downward shift. Therefore, in this

case, the gap was found to become wider when the oscillating turbine is moving upwards; whereas, it was found to become narrower when the floating turbine is moving downwards (see Figure (44b) and Figure (44c)).

The absolute dynamic effects induced by the continuous heaving motion were observed when the oscillating turbine is at the center (the neutral location). The wake profiles were found to shift upwards/downwards when the oscillating turbine is moving downwards/upwards (see Figure (38b) and Figure (38c)). The wake deflection due to the dynamic effects could be linked with the frequency of the heave motion. As the frequency of this up and down motion increases, these dynamic effects would be more pronounced; therefore, the wake deflections would play an important role in the wake development.

Figure (39, 42, and 45) show the pairwise (i.e., moving *upwards* and *downwards*) contour plots of the averaged normalized kinetic energy flux profiles in the wake of the oscillating turbine at different vertical positions. The vertical kinetic energy fluxes are very crucial for the wake recovery as it entrains high momentum flow into the wake. As shown in Figure (39b, 39c, 42b, 42c, and 45b, 45c), negative values of kinetic fluxes were observed in the top tip (shear) layer of the floating turbine, and the areas covered by these negative fluxes were found to expand slowly as the wake flow advects downstream for the floating turbine. The negative valued kinetic energy fluxes could be used as an indicator of the flow entrained into the wake centerline. Therefore, the high momentum flow above the shear layer could mix with the wake flow characterized by greater velocity deficits, thereby accelerate the wake recovery. As a result, downstream turbines in wind farms/arrays could extract more energy from the disturbed flow. It has also been shown by Cal et.al. (2010) that the energy extracted from the turbines inside a wind farm is on the same order of magnitude with these turbulent kinetic energy fluxes.

Figure (39b, 39c, 42b, 42c, and 45b, 45c) also shows the effect of the hysteresis on the development of the kinetic energy fluxes for the floating turbine at predetermined vertical positions. The region with strong/negative fluxes, representing the wake shear (viscous) layer, was found to deflect downwards/upwards if the turbine is moving upwards/downwards. This is parallel to the previous findings on the relation between the wake deflection and the direction of the heave motion. Therefore, in case of a continuous heaving (up and down) motion of an oscillating wind turbine, shear layer expansion would occur in both vertical directions. This could enhance and promote strong mixing in the wake which leads to a faster wake recovery rate. Furthermore, the direction and the speed of the wake expansion strongly depend on the direction and the frequency of the heaving motion, respectively.

The static effects (due to the changes in the hub height of the oscillating turbine) of heaving motion were observed in Figure (39a, 39d, 42d, 45d), and comparisons could be made between the fixed turbine and the oscillating turbine. As shown in Figure (39d, 42d, 45d), the kinetic energy flux profiles were found to be pretty similar for all these cases. This might be attributed to the narrow range (i.e., ± 2 cm) of the heave motion where wind shear does not play a significant role.

As shown in Figure (40, 43, 46), the distribution pattern of the TKE production contours would seem quite similar to the kinetic energy flux contours shown in Figure (39, 42, and 45) It was observed from these figures that higher levels of TKE production, analogous to kinetic energy flux distribution, would occur at the top tip height and behind the nacelle. The maximum TKE production behind the nacelle of the oscillating turbine were found to be comparably higher than those observed at the top tip level. However, TKE production behind the nacelle were found to decay much faster (decays before $x/D = 1.0$) with increasing downstream distance.

The TKE production at the top tip level was observed to spread (i.e., more pronounced after x/D = 1.2) as the flow convects downstream. This spread (i.e., due to the shear layer expansion) can be clearly seen for all the cases. The hysteresis loop, shown in Figure (40b, 40c, 43b, 43c, 46b, 46c) as pairwise (i.e. moving *upwards* and *downwards*) for the specific heights of the oscillating wind turbine, was found to make no significant impacts on the magnitude ranges of TKE production. In addition, the wake deflection due to the hysteresis effects cannot be identified from the TKE production plots. This can be associated with the measurement plane extending only up to a downstream distance of x/D = 1.8 so that shear layer expansion was not fully visualized.

Figure (40a, 40d, 43d, 46d) also displays the static effects (i.e., due to the change in the hub height of the floating turbine) of the heave motion on TKE production profiles in comparison to the fixed turbine. Analogous to the kinetic energy flux profiles, TKE production profiles do not show significant differences (with slight fluctuations in the magnitude) for the fixed turbine and the floating turbine cases.
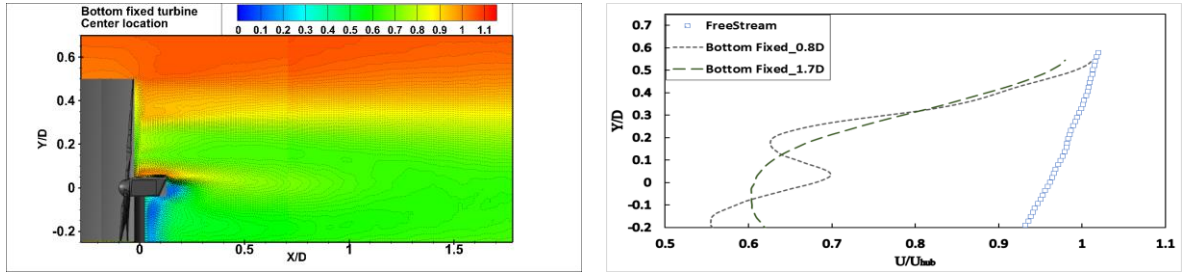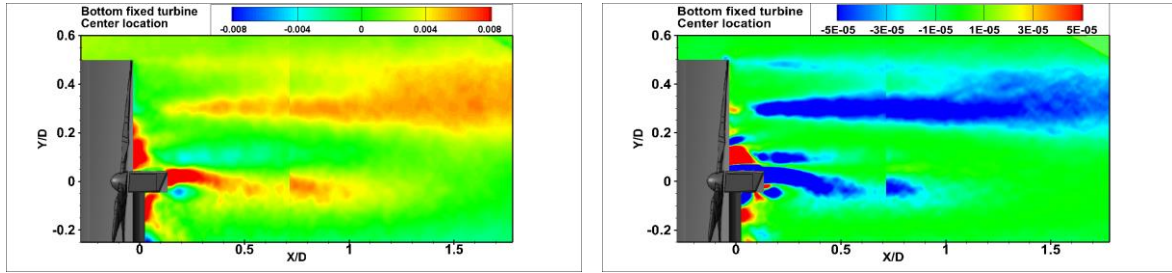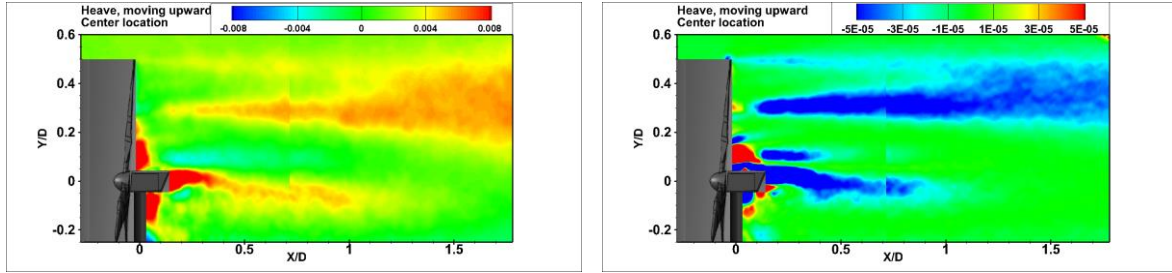
(a) Bottom Fixed Turbine – U/Uhub – Center location
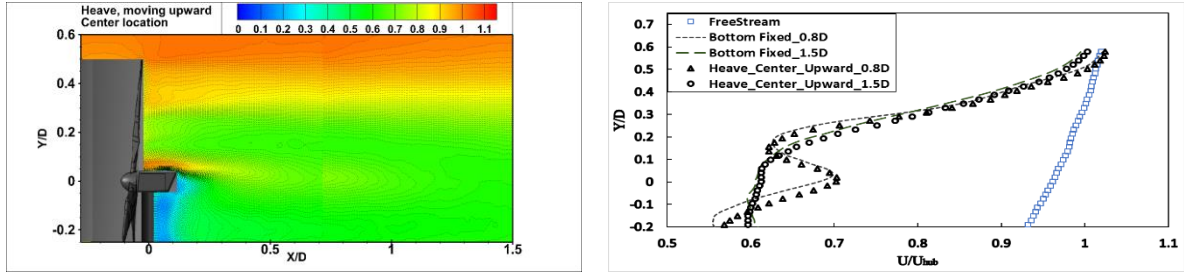
(b) Heave Motion – U/Uhub – Center location – Moving Upward (↑)
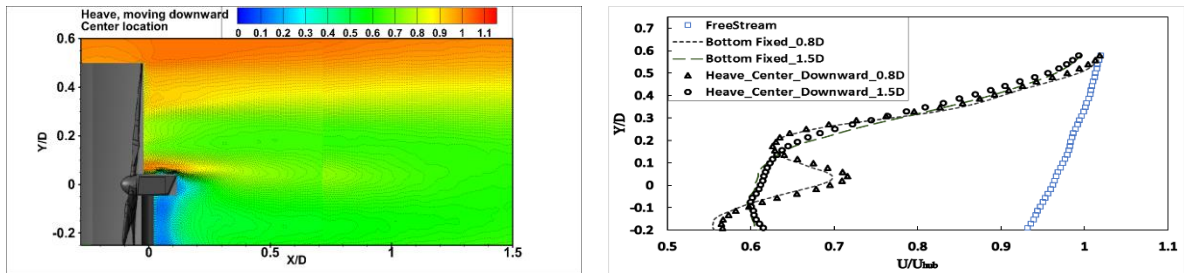
(c) Heave Motion – U/Uhub – Center location – Moving Downward (↓)
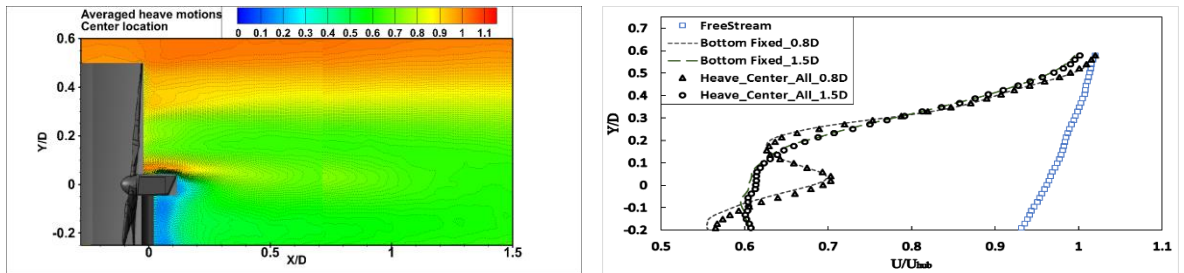
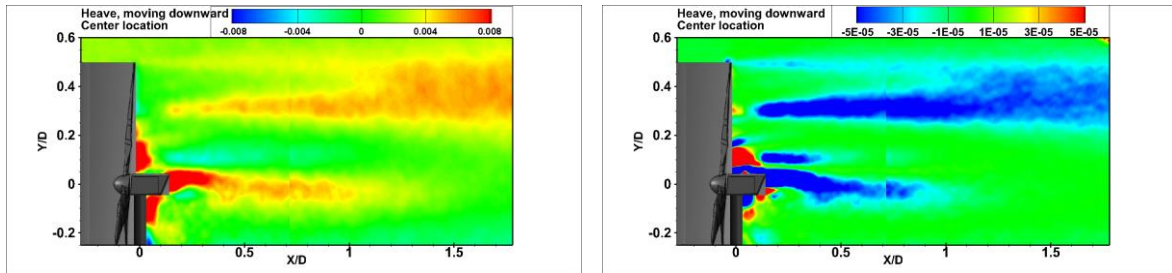(d) Heave Motion – U/Uhub – Center location – Averaged motion

Figure 38: Normalized stream-wise velocity (U/Uhub) profiles in the wake of a bottom fixed turbine (a), the center location for a heaving turbine as it is moving upward (b), as it is moving downward (c), and the averaged of downward and upward motions (d).
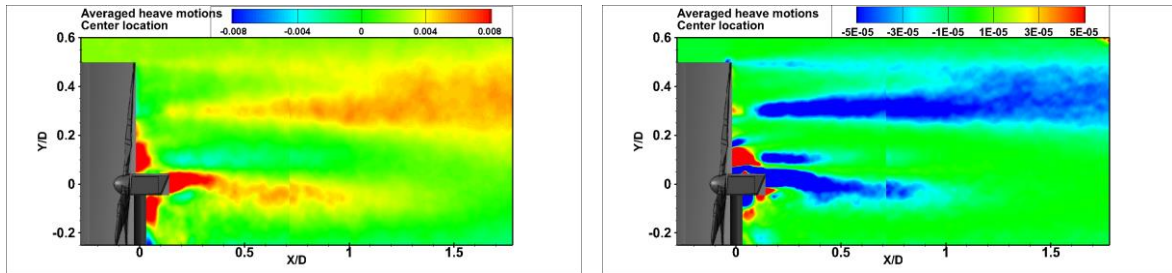
(a) Bottom Fixed Turbine – Reynolds Shear Stress and Momentum Flux – Center location

(b) Heave Motion–Reynolds Shear Stress and Momentum Flux–Center location–Moving Upward (↑)


**(c) Heave Motion–Reynolds Shear Stress and Momentum Flux–Center location–Moving Downward (↓)**

**(d) Heave Motion–Reynolds Shear Stress and Momentum Flux–Center location–Averaged Motion**

Figure 39: Normalized Reynolds Shear Stress ($\frac{Ruv}{U_{hub}^2}$) and the Momentum Flux ($\frac{\frac{\partial U}{\partial Y}*Ruv*D}{U_{hub}^3}$) plots in the wake of a bottom fixed turbine (a), and the center location of a heaving turbine as it is moving upward (b), as it is moving downward (c), and the averaged of downward and upward motions (d).
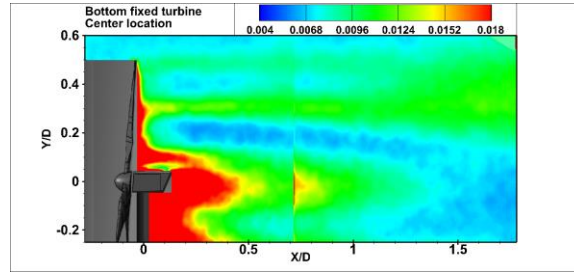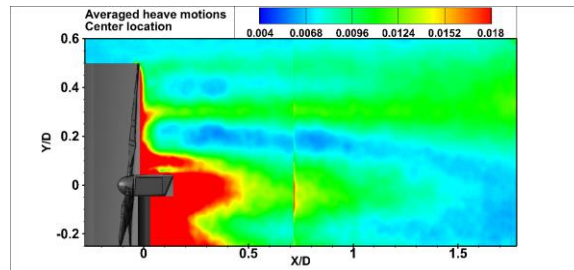
(a) Bottom Fixed Turbine – Center location – T.K.E.
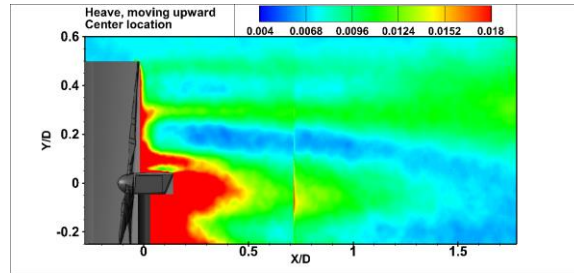
(b) Heave Motion – Center location – Moving Upward – T.K.E. (↑)
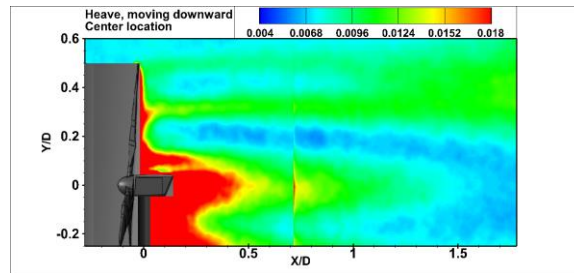
(c) Heave Motion – Center location – Moving Downward – T.K.E. (↓)

(d) Heave Motion – Center location – Averaged Motion – T.K.E.

Figure 40: Normalized Turbulent Kinetic Energy ($\frac{T.K.E.}{U_{hub}^2}$) plots in the wake of a bottom fixed turbine (a), and the center location of a heaving turbine as it is moving upward (b), as it is moving downward (c), and the average of downward and upward motions (d).
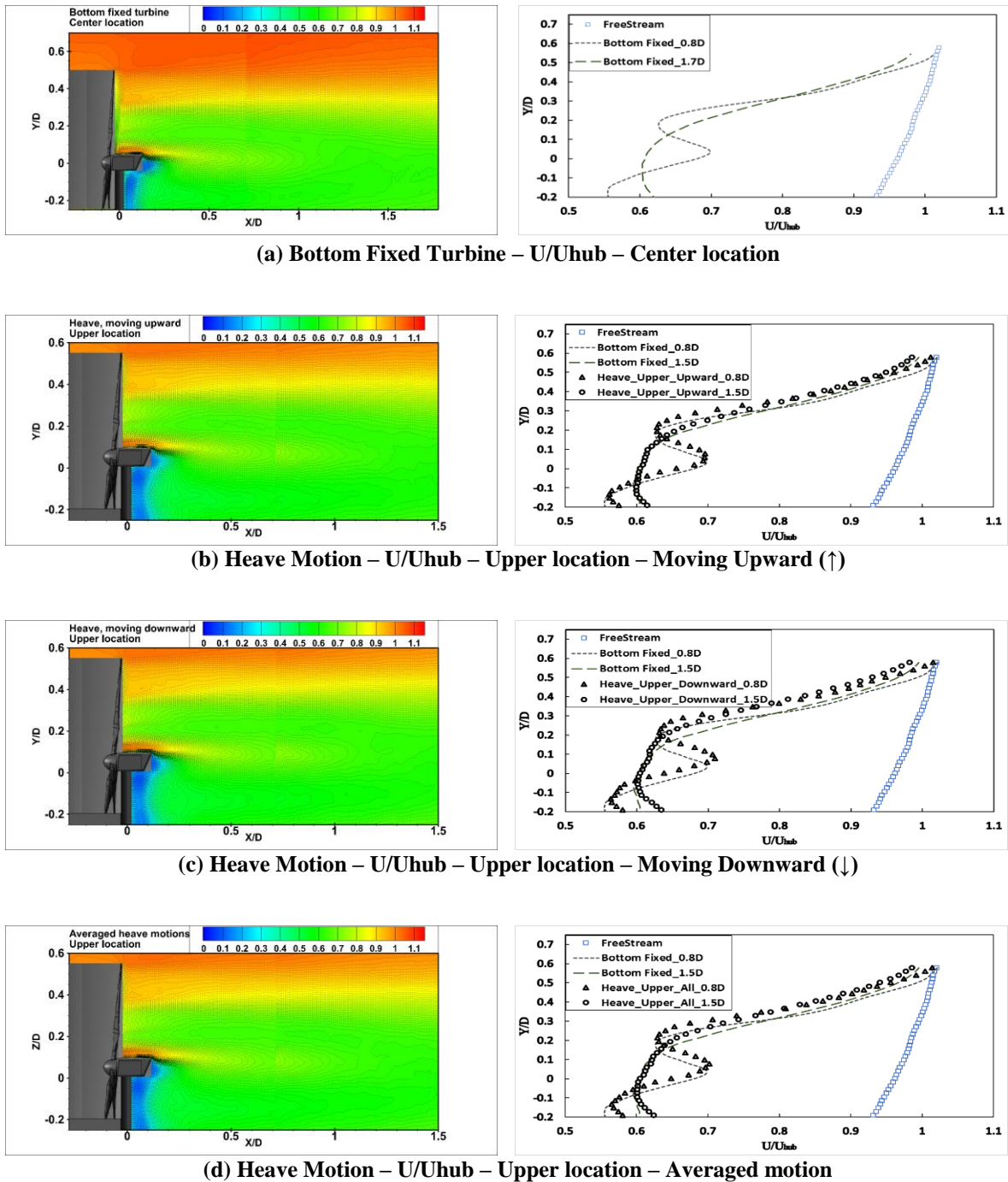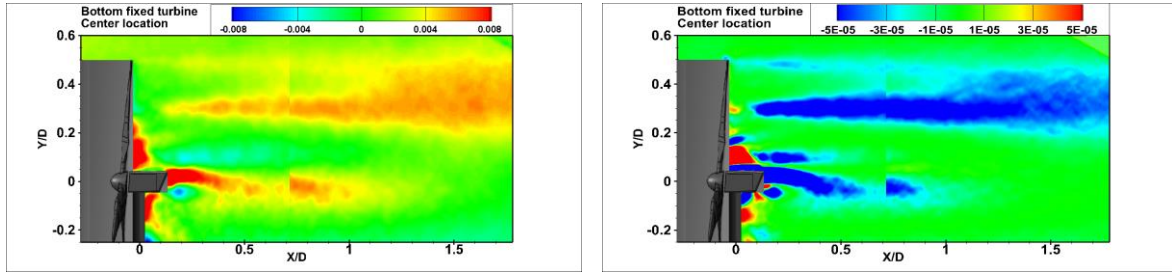
(a) Bottom Fixed Turbine – U/Uhub – Center location

(b) Heave Motion – U/Uhub – Upper location – Moving Upward (↑)

(c) Heave Motion – U/Uhub – Upper location – Moving Downward (↓)

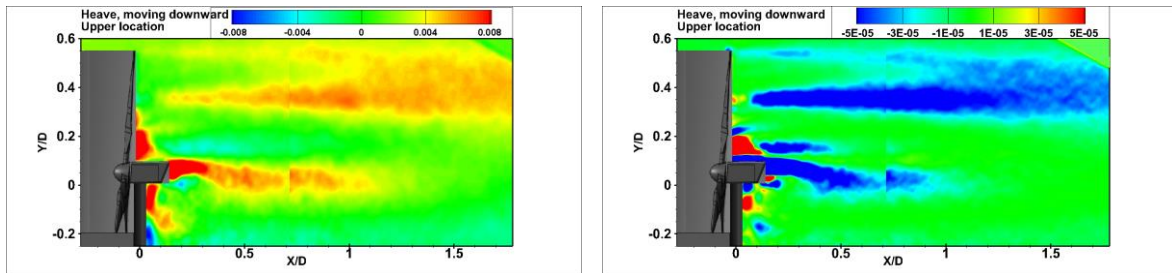(d) Heave Motion – U/Uhub – Upper location – Averaged motion

Figure 41: Normalized stream-wise velocity (U/Uhub) profiles in the wake of a bottom fixed turbine (a), the upper location for a heaving turbine as it is moving upward (b), as it is moving downward (c), and the averaged of downward and upward motions (d).
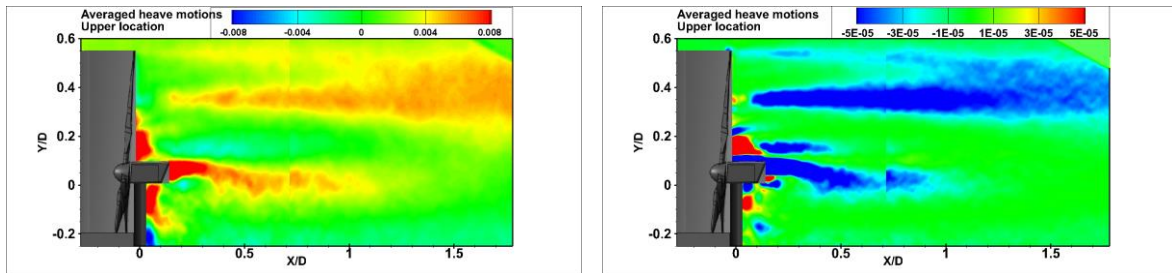
(a) Bottom Fixed Turbine – Reynolds Shear Stress and Momentum Flux – Center location
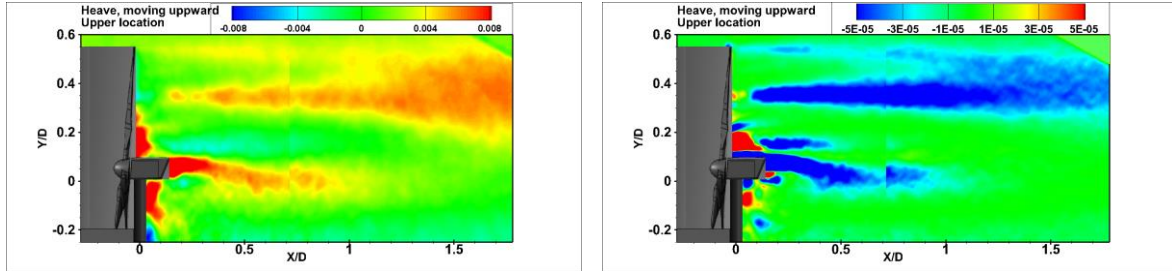
(b) Heave Motion–Reynolds Shear Stress and Momentum Flux–Upper location–Moving Upward (↑)


(c) Heave Motion–Reynolds Shear Stress and Momentum Flux–Upper location–Moving Downward (↓)


(d) Heave Motion–Reynolds Shear Stress and Momentum Flux–Upper location–Averaged Motion

Figure 42: Normalized Reynolds Shear Stress ($\frac{Ruv}{U_{hub}^2}$) and the Momentum Flux ($\frac{\frac{\partial U}{\partial Y}*Ruv*D}{U_{hub}^3}$) plots in the wake of a bottom fixed turbine (a), and the upper location of a heaving turbine as it is moving upward (b), as it is moving downward (c), and the averaged of downward and upward motions (d).
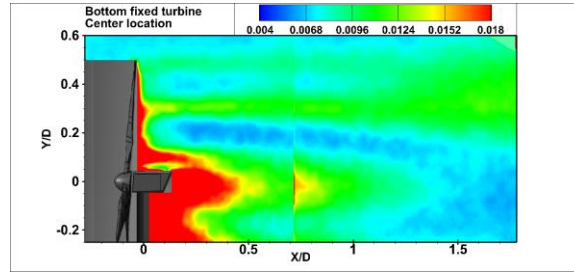
(a) Bottom Fixed Turbine – Center location – T.K.E.
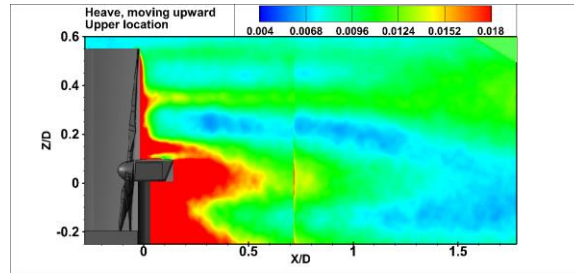
(b) Heave Motion – Upper location – Moving Upward – T.K.E. (↑)
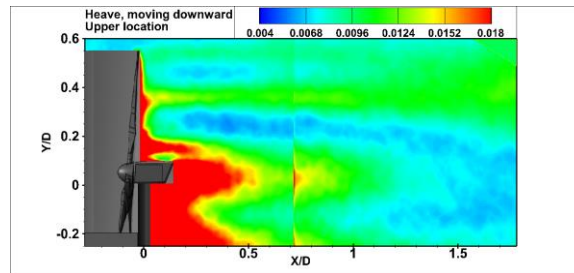
(c) Heave Motion – Upper location – Moving Downward – T.K.E. (↓)

(d) Heave Motion – Upper location – Averaged Motion – T.K.E.

Figure 43: Normalized Turbulent Kinetic Energy ($\frac{T.K.E.}{U_{hub}^2}$) plots in the wake of a bottom fixed turbine (a), and the upper location of a heaving turbine as it is moving upward (b), as it is moving downward (c), and the average of downward and upward motions (d).
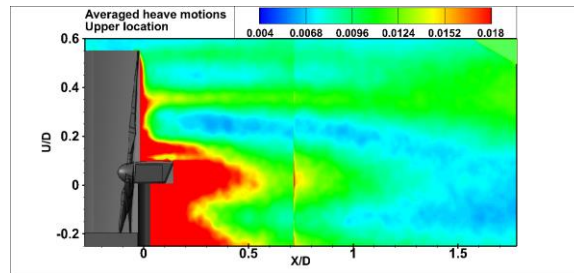
(a) Bottom Fixed Turbine – U/Uhub – Center location

(b) Heave Motion – U/Uhub – Lower location – Moving Upward (↑)

(c) Heave Motion – U/Uhub – Lower location – Moving Downward (↓)
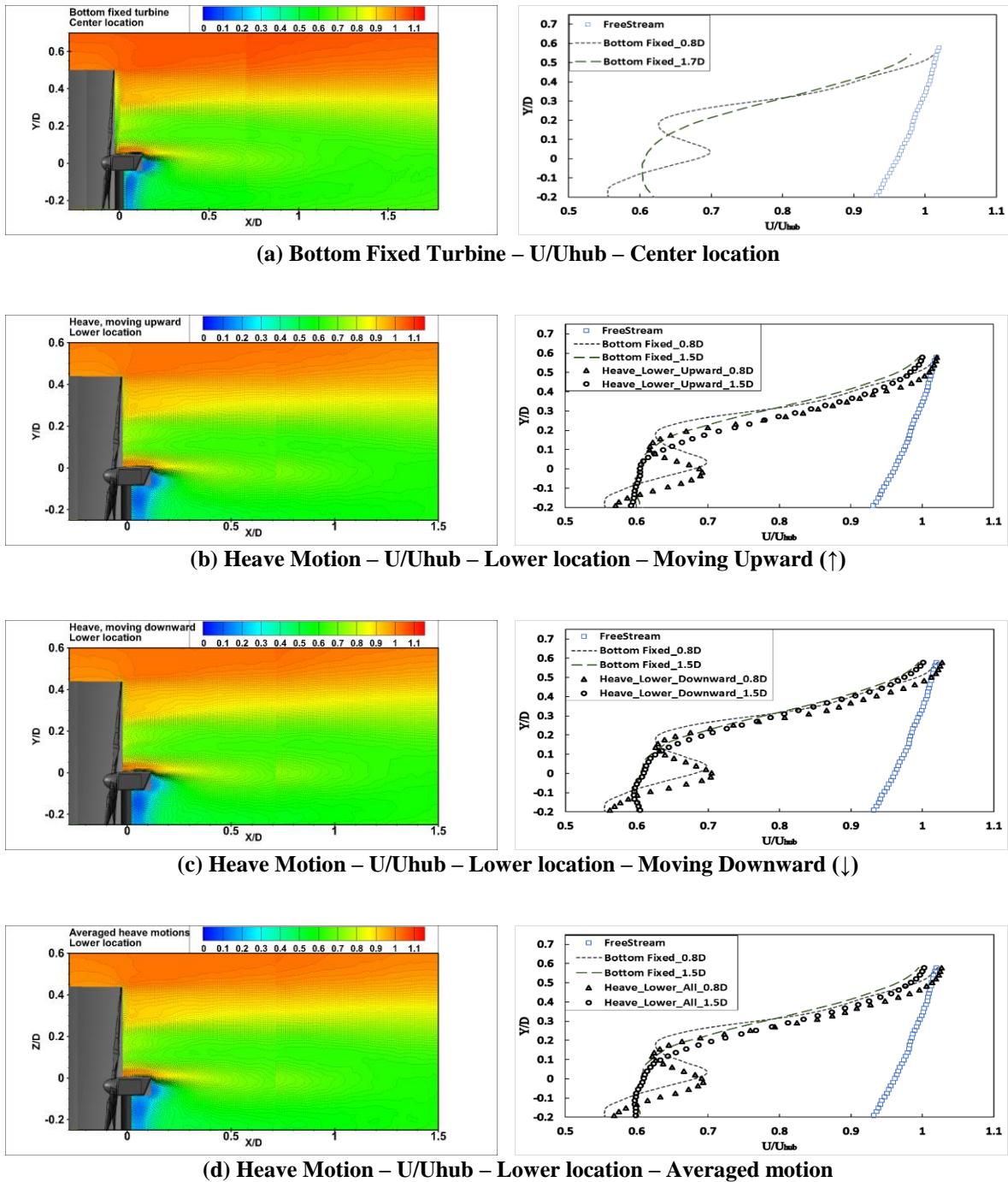

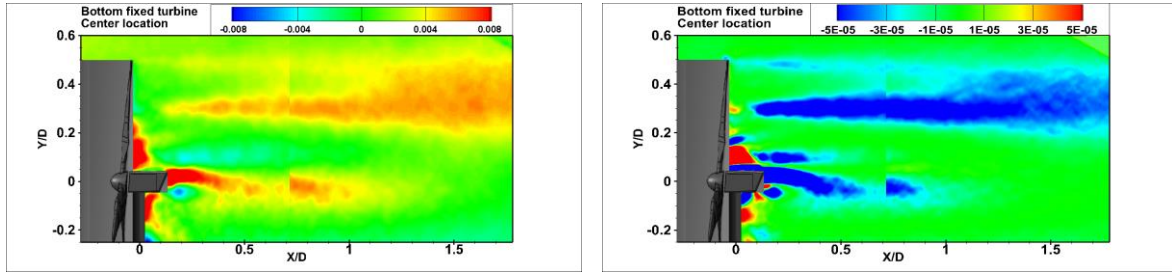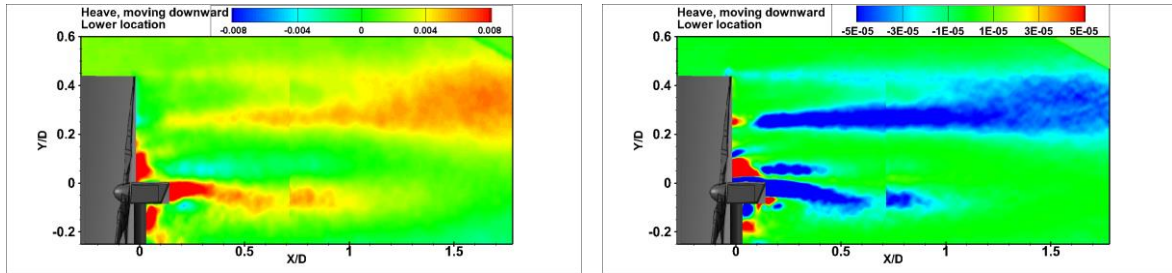**(d) Heave Motion – U/Uhub – Lower location – Averaged motion**

Figure 44: Normalized stream-wise velocity (U/Uhub) profiles in the wake of a bottom fixed turbine (a), the lower location for a heaving turbine as it is moving upward (b), as it is moving downward (c), and the averaged of downward and upward motions (d).

(a) Bottom Fixed Turbine – Reynolds Shear Stress and Momentum Flux – Center location
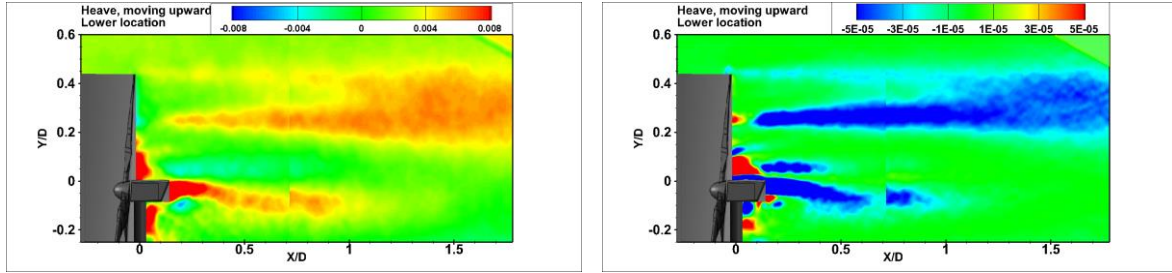
(b) Heave Motion–Reynolds Shear Stress and Momentum Flux–Lower location–Moving Upward (↑)

(c) Heave Motion–Reynolds Shear Stress and Momentum Flux–Lower location–Moving Downward (↓)
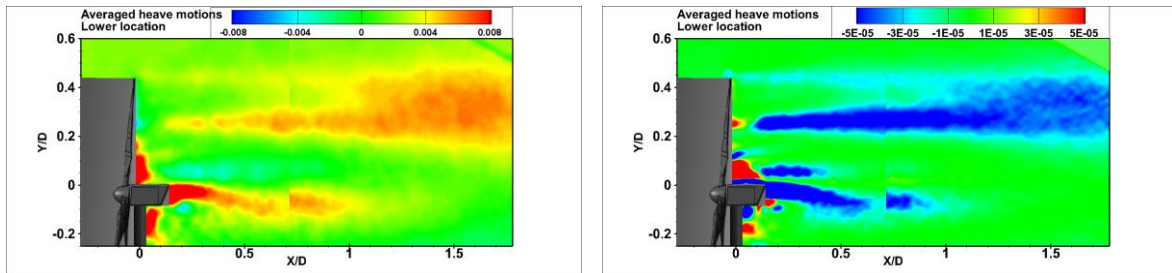
(d) Heave Motion–Reynolds Shear Stress and Momentum Flux–Lower location–Averaged Motion

Figure 45: Normalized Reynolds Shear Stress ($\frac{Ruv}{U_{hub}^2}$) and the Momentum Flux ($\frac{\frac{\partial U}{\partial Y}*Ruv*D}{U_{hub}^3}$) plots in the wake of a bottom fixed turbine (a), and the lower location of a heaving turbine as it is moving upward (b), as it is moving downward (c), and the averaged of downward and upward motions (d).
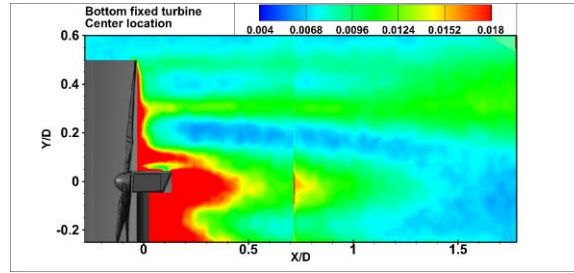
(a) Bottom Fixed Turbine – Center location – T.K.E.
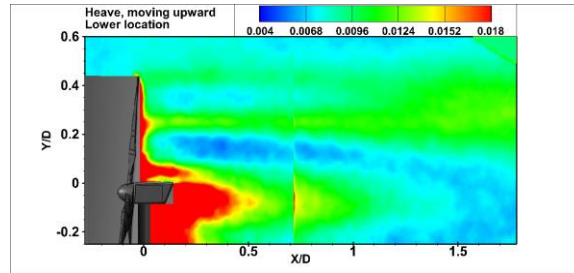
(b) Heave Motion – Lower location – Moving Upward – T.K.E. (↑)
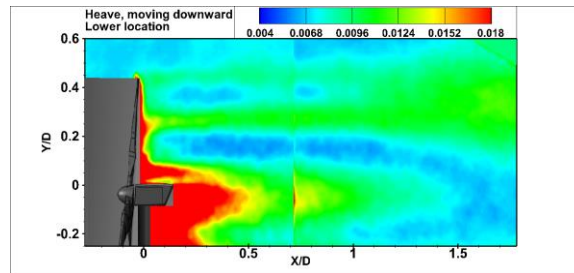
(c) Heave Motion – Lower location – Moving Downward – T.K.E. (↓)
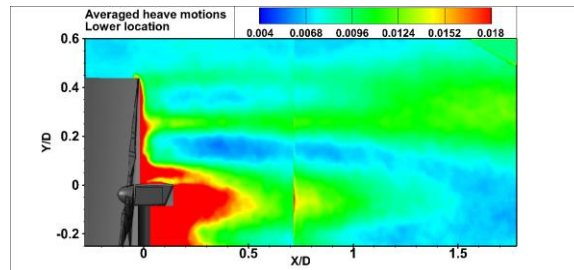
(d) Heave Motion – Lower location – Averaged Motion – T.K.E.

Figure 46: Normalized Turbulent Kinetic Energy ($\frac{T.K.E.}{U_{hub}^2}$) plots in the wake of a bottom fixed turbine (a), and the lower location of a heaving turbine as it is moving upward (b), as it is moving downward (c), and the average of downward and upward motions (d).

CHAPTER 3

CONCLUDING REMARKS

3.1 General Conclusions

Offshore floating wind turbines are the future of wind energy (Sebastian et al., 2013). The United States is especially fortunate to be surrounded by vast yet deep waters on both sides of the nation. This provides a unique opportunity for offshore floating wind farm developments in this country. But, so far, no major progress has been made in developing any offshore floating wind farms. This is mainly due to lack of experience and knowledge needed to overcome the obstacles faced by wind turbine manufacturers. One of these obstacles is the uncertainty associated with the performance and sitting of such floating turbines. With only few numerical simulation studies being done to understand the coupled behavior of floating offshore wind turbines, there is a need for a comprehensive experimental study to validate the numerical results and perhaps to improve our current understanding of the floating offshore wind turbines' performance and aerodynamics, which can potentially lead to more accurate load and performance predictions and design improvements.

In order to understand, and fully explore the aeromechanics behavior of a floating wind turbine, a comprehensive experimental study was conducted on a wind turbine subjected to uncoupled base motions: surge, pitch, and heave. The results were then compared to that of a classical bottom fixed turbine. These studies were performed under the condition of normal sea condition and therefore, no extreme scenarios were evaluated in this study. A high resolution PIV system was used for detailed near wake flow field measurements (free-run) so as to quantify the near wake turbulent flow structures. The results of the wake study

however, shows strong dependency on which direction the turbine is oscillating. In the case of the surge motion, the wake velocity neither accelerated nor decelerated to any noticeable amount, when compared to the wake of a bottom fixed turbine. Hence, the power measurement of the turbine in surge motion will likely be very similar to that of the bottom fixed turbine. However, as the turbine was moving into the flow, an increase in both the entrainment of the turbulent kinetic energy, and the production of the Reynolds shear stress were observed. But, as the turbine moved with the flow, a decrease in the entrainment of the turbulent kinetic energy, as well as a reduction in the production of the Reynolds shear stress was observed when compared to the wake of a traditional bottom-fixed turbine.

The effects of the pitching motion as well as the hysteresis loop on the mean and turbulent quantities were also investigated. The effects of the hysteresis loop were found to be comparably very small when compared with the effects of the pitching motion. The measurements behind the pitching turbine were then compared with those behind the fixed turbine. Thus, pitch motion of the floating turbine was found to result in significant changes in the wake which provides invaluable information about the future of the offshore wind energy applications. This study would then be extended to study how these changes in the wake of the floating turbine could affect the loads experienced by the downstream turbines as well as their energy generation.

The static and dynamic effects of the heaving motion on the mean and turbulent quantities were investigated. The wake development behind the oscillating turbine in pure heave motion was found to be altered by the direction of the heave motion (hysteresis effect). This study would then be extended to study how these changes in the wake of the floating turbine could be influenced by the vertical range and frequency of the heave motion. It is also crucial to

investigate how the downstream turbines behind the floating turbines can be affected in terms of the power output performance and dynamic loading.

It is also important to mention that the results of the wake study, performance, and the loading are heavily dependent on the velocity and the frequency of oscillation.

BIBLIOGRAPHY

Sebastian, T.; Lackner, M. Characterization of the unsteady aerodynamics of offshore floating wind turbines. Wind Energy 2013, 16, 339–352.

Rockel, S.; Camp, E.; Schmidt, J.; Peinke, J.; Cal, R.B.; Hölling, M. Experimental Study on Influence of Pitch Motion on the Wake of a Floating Wind Turbine Model. Energies 2014, 7, 1954-1985.

Vermeer LJ, Sorensen JN, Crespo A (2003) Wind turbine wake aerodynamics. Prog Aerosp Sci 39:467–510

Massouh H, Dobrev I (2007) Exploration of the vortex behind of wind turbine rotor. J Phys Conf Ser 75:012036

Chamorro, L. P., Porte-Agel, F. (2009). A wind-tunnel investigation of wind-turbine wakes: boundary layer turbulence effects. Boundary Layer Meteorol 132:129–149

Porte-Agel, F., Wu, Y. T., Lu, H., Conzemius, R. J. (2011). Large-eddy simulation of atmospheric boundary layer flow through wind turbines and wind farms. Journal of Wind Engineering and Industrial Aerodynamics, 99, 154–168.

Zhang, W., Markfort, C. D., Porte-Agel, F. (2012). Near-wake flow structure downwind of a wind turbine in a turbulent boundary layer. Experiments in Fluids, 52, 1219–1235.

Hu, H., Yang, Z., Sarkar, P., (2012). Dynamic Wind Loads and Wake Characteristics of a Wind Turbine Model in an Atmospheric Boundary Layer Wind. Experiments in Fluids 52(5):1277-1294.

Wu, Y. T. & Porte-Agel, F. (2012). Atmospheric turbulence effects on wind-turbine wakes: An LES study. Energies, 5, (12), 5340–5362.

Musial W., Ram B., 2010, Large-Scale Offshore Wind Power in the United States, Technical Report NREL/TP-500-40745.

Martin H.R., 2011, Development of a Scale Model Wind Turbine for Testing of Offshore Floating Wind Turbine Systems, M.S. Thesis, University of Maine, Orono.

Wieringa, J (1992). Updating the Davenport roughness classification. Journal of Wind Engineering and Industrial Aerodynamics 41-44, 357-386.

Manwell, J. F., McGowan, J. G., & Rogers, A. L. (2010). Wind Energy Explained: Theory, Design and Application, 2nd edition. Wiley.

Hau, E. Wind Turbines Fundamentals, Technologies, Application, Economics, 2nd edition. Springer

A. Ozbay, W. Tian, Z. Yang, and H. Hu, "An experimental investigation on the wake interference of multiple wind turbines in atmospheric boundary layer winds," in AIAA-2012-2784, 30th AIAA Applied Aerodynamics Conference, New Orleans, Louisiana, 25-28 June 2012

Corbetta, G., Mbistrova, A. 2015, The European offshore wind industry key trends and statistics 2014, EWEA.

K. S. Hansen, R. J. Barthelmie, L. E. Jensen, and A. Sommer, "The impact of turbulence intensity and atmospheric stability on power deficits due to wind turbine wakes at Horns Rev wind farm," Wind Energy 15, 183–196 (2012).

Sanderse, B. (2009). Aerodynamics of wind turbine wakes: Literature review. Energy Research Center of the Netherlands (ECN).

Lignarolo, L.E.M., Ragni, D. Krishnaswami, C., Chen, Q., Simao Ferreira, C. J., & Van Bussel, G.J.W. (2013). Experimental analysis of the kinetic energy transport and turbulence production in the wake of a model wind turbine. ICOWES Conference, Lyngby, 16-19 June.

Architecture Institute of Japan, AIJ Recommendations for Loads on Buildings (Architectural Institute of Japan, 1996).

Barthelmie, R. and Jensen, L. E. (2010). Evaluation of the wind farm efficiency and wind turbine wakes at the Nysted offshore wind farm. Wind Energy, 13:573-586. Doi:10.1002/we.408

Barthelmie, R. J., Hansen, K., Frandsen, S.T., Rathmann, O., Schepers, J.G., Schlez, W., et al. (2009). Modeling and measuring flow and wind turbine wakes in large wind farms offshore. Wind Energy 12(5), 431-444. Doi:10.1002/we.348.

Meyers, J., & Meneveau, C. (2013). Flow visualization using momentum and energy transport tubes and applications to turbulent flow in wind farms. Journal of Fluid Mechanics 715, 335-358.

J.M. Jonkman, (2007). Dynamics Modeling and Loads Analysis of an Offshore Floating Wind Turbine Technical Report NREL/TP-500-41958

Cal, R. B., Lebron, J., Castillo, L., Kang, H.S., Meneveau, C. (2010). Experimental study of the horizontally averaged flow structure in a model wind-turbine array boundary layer. J Renew sustain Energy 2:013-106.